이학박사 학위논문

Investigation of the atmospheric impacts of gas/particle phase organic chemistry in Korea

대기 중 가스상/입자상 유기화학 과정이 국내 대기환경에 미치는 영향 연구

2023년 2월

서울대학교 대학원

지구환경과학부

옥 유 진

Investigation of the atmospheric impacts of gas/particle phase organic chemistry in Korea

지도 교수 박 록 진

이 논문을 이학박사 학위논문으로 제출함

2022년 10월

서울대학교 대학원

지구환경과학부

옥 유 진

옥유진의 이학박사 학위논문을 인준함

2023년 1월

위 원 장 _____ (인)

부위원장 _____ (인)

위 원 _____ (인)

위 원 _____ (인)

위 원 _____ (인)

Abstract

Air pollution in Korea calls for efforts on the assessment of the atmospheric impacts of gas and particle phase organic chemistry, which can form major air pollutants including tropospheric ozone (O_3) and fine particulate matter ($PM_{2.5}$). Long-term exposure to these pollutants can cause severe diseases in the human cardiovascular and respiratory systems. Here I investigated the effect of gas phase organic chemistry on tropospheric O_3 and oxidants in Korea, focusing on aromatic volatile organic compounds (VOCs), which are abundant reactive species in East Asia. Using a 3-D chemical transport model (CTM), GEOS-Chem, I found that implementing a detailed aromatic chemistry mechanism increases daytime O_3 concentrations by 13% in Korea. Evaluation of the simulated O_3 production efficiency with updated chemistry implies that nitrogen oxide (NO_x) emissions are underestimated in the bottom-up emissions inventory. Sensitivity tests showed that O_3 levels increase in urban areas with reductions in domestic NO_x emissions, but with simultaneous reductions in both NO_x and VOCs emissions O_3 decreases in most regions. I also investigated the chemical formation and loss processes of organic aerosols (OA) by comparing different secondary organic aerosol (SOA) simulation schemes using GEOS-Chem. I examined the characteristics of SOA formation in Seoul during different seasons and found that the inclusion of semi/intermediate VOCs (S/IVOCs) precursors and SOA aging are important features in the model. This analysis provides a comparison of

the scientific understandings embedded in each SOA scheme and the best suitable approach in simulating OA in a typical urban environment in Korea. Finally, based on model evaluation and analysis on gas/particle phase organic chemistry, I investigated the future changes in air quality in Korea and its health impacts under the Shared Socioeconomic Pathways (SSPs). I utilized the updated aromatic chemistry and best-performing SOA scheme to simulate the present, near-term, and long-term future air quality, along with concentration response factors (CRFs) obtained from Korean epidemiologic studies to estimate air pollution attributable premature mortality. The updated aromatic chemistry was responsible for a ~21% increase in estimated premature mortality in Korea during the springtime in 2016. Under SSP1, successful reductions on anthropogenic emissions will largely improve air quality in Korea, and the resulting cardiovascular premature mortality will significantly decrease (−95%) in the long-term future, and the health impact of biogenic SOA will become more important than other species. Under SSP3, air pollution attributable premature mortality will decrease by 22% in the long-term compared to present, but the changes in SOA concentrations will cause a ~20% increase in SOA-attributable cardiorespiratory deaths.

Keywords: Chemical Transport Model, Volatile Organic Compounds, Ozone, Organic Aerosols, $PM_{2.5}$, Air quality, Premature mortality

Student Number: 2016-23700

Table of Contents

List of Figures

List of Tables

Chapter 1. Introduction

Atmospheric organic compounds, including various kinds of liquid/gas/particle phase species in the atmosphere that contain carbon, are ubiquitous compounds emitted from both natural and anthropogenic sources (e.g., vegetation, fossil fuel, biomass, etc.) which differ in chemical/physical properties such as reactivity and volatility (Glasius and Goldstein, 2016). Once emitted, organic vapors are oxidized, for example by the hydroxyl radical (OH), and their reactivities typically increase with increasing carbon (C) and oxygen (O) number, but can also decrease depending on the O:C ratio (Donahue *et al.*, 2013). Organic compounds can also be classified as VOCs (volatile organic compounds), IVOCs (intermediate volatility organic compounds), SVOCs (semivolatile organic compounds), LVOCs (low volatility compounds), etc., by their volatilities (Donahue *et al.*, 2013). These compounds are meta-stable and can exist in both gas and particle phases depending on their effective saturation mass concentration (C^*) and the partitioning theory (Donahue *et al.*, 2006).

Sources and the atmospheric fates of organic compounds are important because not only can they can form tropospheric ozone (O_3) and fine particulate matter ($PM_{2.5}$), but also can modulate the oxidation capacity of the atmosphere and can affect the ambient levels of other major air pollutants, including nitrogen oxides (NO_x) and sulfur dioxide (SO_2). Adverse health effects of long-term exposure to these surface air pollutants on the human

cardiovascular and respiratory systems have been widely addressed by epidemiologic (Hoek *et al.*, 2013; Faustini, Rapp and Forastiere, 2014; Crouse *et al.*, 2015; Huangfu and Atkinson, 2020; Soares and Silva, 2022) and air quality modeling studies (Anenberg *et al.*, 2010; Silva *et al.*, 2016; Xu *et al.*, 2021). Therefore, scientific understanding of atmospheric organic compounds is essential in investigating the causes and potential impacts of air pollution and establishing control strategies for the future, especially in terms of adaptation and mitigation of future climate change.

The gas phase chemistry of organics is essential to the formation of O_3, which is a toxic pollutant to both human and ecosystem (https://www.epa.gov/ground-level-ozone-pollution). O_3 in the troposphere is photochemically produced from the oxidation of VOCs in the presence of NO_x ($\equiv NO + NO_2$) (World Health Organization, 2003). VOCs also serve as the precursors of particle phase organic aerosols (OA), which represent a large fraction (20−90%) of total submicron particulate matter (PM_1) globally (Zhang *et al.*, 2007; Zhou *et al.*, 2020). While primary organic aerosols (POA) can be directly emitted from combustion sources, the oxidation of VOCs and chemical processing can additionally form secondary organic aerosols (SOA) (Chacon-Madrid and Donahue, 2011).

Although numerous studies on atmospheric organic chemistry using various tools including observations and models provide insight to the role of organic compounds (Glasius and Goldstein, 2016), large uncertainties in

model parametrizations and unknown processes still call for efforts to fill the gaps between the real atmosphere and current scientific understanding.

Air quality assessment and research are of great interest in East Asia, including Korea, recently, as global distributions and trends of pollutant concentrations show that not only is East Asia one of the major air pollution hotspots in the Northern hemisphere (Shaddick *et al.*, 2018; Chang *et al.*, 2019), but also annual O_3 change and $PM_{2.5}$ exposure in East Asia have increased during the past two decades (Wang *et al.*, 2016). East Asia also ranked first in the world in estimated deaths during 2015 caused by transportation-attributable O_3 and $PM_{2.5}$ (Anenberg *et al.*, 2019).

Recently, during the past three years, ongoing reduction policies on Northeast Asian anthropogenic emissions and the outbreak of COVID-19 have resulted in a decrease in precursor concentrations (Ju, Oh and Choi, 2021). However, the impact on O_3 and $PM_{2.5}$ do not appear to be linear to the changes in precursor emissions (Ju, Oh and Choi, 2021). Local emission characteristics of VOCs and NO_x may create a unique environment for organic chemistry and secondary pollutant formation (Park and Kim, 2014). Along with concentrated NO_x levels, particularly high levels of aromatics including toluene and xylenes were observed in Seoul (Khan *et al.*, 2018; Simpson *et al.*, 2020; Wang *et al.*, 2021). This emphasizes the need for comprehensive and quantitative analysis based on regional characteristics to understand the nature of atmospheric chemistry in this region.

Chemical transport models (CTMs) have been used as an effective tool for testing the atmospheric response to changes in pollutant emissions, chemistry, and their fates (Carmichael *et al.*, 2008). Simulated O_3 and OA concentrations in East Asia have generally been underestimated in CTMs (Han *et al.*, 2008; Park *et al.*, 2021), and relatively coarse model resolutions have been limitations of previous studies (Jo *et al.*, 2013; Pai *et al.*, 2020). This dissertation examines the characteristics and sources of O_3 and OA formation focusing on organic chemistry in urban environments in Korea using a 3-D global CTM, GEOS-Chem. To understand the atmospheric role of gas/particle phase organic chemistry in determining air quality and to assess the future impacts of organic compounds in Korea, this dissertation investigates the following topics.

1. Effect of gas phase organic chemistry on tropospheric O_3 and oxidants (Chapter 2)
2. Chemical/physical formation and loss processes of organic aerosols (Chapter 3)
3. Future changes and health impacts of organic compounds (Chapter 4)

Chapter 2. Effect of gas phase organic chemistry on tropospheric ozone (O_3) and oxidants

The Korean government has adopted regulations on major emission sectors including mobile and industrial sources since the 1990s (Kim and Lee, 2018). As a result, both VOCs and NO_x emissions and ambient concentrations have continuously decreased in Seoul (Kim and Lee, 2018), but O_3 concentrations show rather an increasing trend. This is because of the non-linear chemical relationship between O_3 and its precursors (VOCs and NO_x). Therefore, instead of ambient O_3 concentrations, an effective metric called the O_3 production efficiency (OPE) can be used to examine the non-linearity of O_3 production (Lin, Trainer and Liu, 1988). The OPE represents the number of O_3 molecules produced per NO_x molecules consumed, and is calculated following Eq. (2.5), using instantaneous rates of O_3 formation (Eq. (2.1), destruction (Eq. (2.2), and NO_x loss (Eq. (2.3).

Eq. (2.1) $F_{O_3} = k_{NO+HO_2}[NO][HO_2] + \sum_i k_{NO+RO_{2_i}}[NO][RO_{2_i}]$

Eq. (2.2) $D_{O_3} = k_{O(^1D)+H_2O}[O(^1D)][H_2O] + k_{O_3+HO_2}[O_3][HO_2] + k_{O_3+OH}[O_3][OH] + \sum_i k_{O_3+VOC_i}[O_3][VOC_i] + k_{NO_2+OH}[NO_2][OH]$

Eq. (2.3) $P_{O_3} = F_{O_3} - D_{O_3}$

Eq. (2.4) $L_{NO_x} = k_{NO_2+OH}[NO_2][OH]$

Eq. (2.5) $OPE = P_{O_3}/L_{NO_x}$

The second term in Eq. (2.1) represents the O_3 formation rate through

VOCs oxidation, implying that the species with high reactivity and high ambient concentrations will be likely to produce more O_3. According to the Korean National Institute of Environmental Research (NIER), roughly half the total non-methane VOCs (NMVOCs) anthropogenic emissions in Korea during 2017 was attributable to solvent use. Solvent use includes activities such as painting, coating, printing, dry cleaning, etc., which typically emit aromatic compounds, which have high reactivities compared to commonly emitted short-chained alkanes (Atkinson, 2000). Among the various VOCs observed during 2015−2016 at Seoul, high levels of aromatics including toluene and xylenes were observed (Khan *et al.*, 2018; Schroeder *et al.*, 2020; Simpson *et al.*, 2020), reflecting the abundance of aromatic VOCs in these regions. Aromatic VOCs also accounted for 44% of observed total VOCs reactivity in Seoul during 2016 (Simpson *et al.*, 2020). Considering its abundance and high reactivity, in this chapter I investigated the role of aromatics in gas phase organic chemistry in Korea during the KORUS-AQ campaign (May−June 2016) using a 3-D CTM.

2.1. Method

2.1.1. KORUS-AQ field campaign

The Korea United States Air Quality (KORUS-AQ) campaign is an international air quality field campaign that was held in Korea, during spring (May 1–June 10) 2016, which was led by NIER and the United States National Aeronautics and Space Administration (NASA) (Crawford *et al.*, 2021). 60-second averaged airborne (DC-8) observations below 1.5 km during photochemically active hours (13:00–16:00 Local Time; LT) of O_3, NO_x, OH, and speciated VOCs onboard the DC-8 aircraft are used in this study.

Time-dependent observation-constrained 0-D photochemical box modeling was conducted by the NASA Langley Research Center (LaRC) to simulate the oxidation and photochemical processes during KORUS-AQ. Model inputs derived from 1-second averaged DC-8 observations of temperature, pressure, photolysis rates, O_3, CO, NO, H_2O_2, CH_3OOH, HNO_3, PAN, HCHO, and VOCs were used as constraints to calculate diurnal steady state concentrations of radical species (Schroeder *et al.*, 2020). Using a customized chemical mechanism with reaction rates based on NASA JPL 2012 and IUPAC 2006 recommendations, concentrations of NO_2, OH, HO_2, RO_2, instantaneous production and loss rates of O_3 and NO_x were calculated. The box model calculations include dry deposition loss, and rainout, but do not include any heterogeneous chemistry and convection. Box model

predictions of NO_2, OH, and peroxy radicals are in good agreements with observations (Schroeder *et al.*, 2020), and therefore I assumed that the observation-constrained box model represents the true atmosphere.

2.1.2. Model configuration

I used GEOS-Chem v10-01 and its nested configuration to simulate gas and aerosol species (Bey *et al.*, 2001) in Korea during KORUS-AQ. The model is driven by the Goddard Earth Observing System forward processing (GEOS-FP) assimilated meteorological field provided by the NASA Global Modeling Assimilation Office (GMAO). Global simulations with 2° × 2.5° horizontal resolutions and one-month spin-ups were conducted prior to nested simulations to provide hourly boundary and initial conditions. The nested configuration covers the East Asian domain (15–55°N, 70–140°E) with 0.25° × 0.3125° horizontal resolutions and 47 vertical layers using hybrid pressure-sigma coordinates (1013.25–0.010 hPa).

The default NO_x-O_3-VOCs chemical mechanism includes abbreviated aromatic chemistry from Henze *et al*. (2008), which does not fully represent the VOCs chemistry in Korea (Table 2.1). To account for the significance of aromatic VOCs, I implemented an updated aromatic chemistry mechanism following the work of Porter *et al*. (2017) to GEOS-Chem. The default aromatic chemistry mechanism was replaced with a total of 37 aromatic-related reactions including kinetic and photolysis reactions, with 7 additional reaction intermediates summarized in Table 2.2.

For emission inputs I used anthropogenic emissions of carbon monoxide (CO), NO_x, SO_2, ammonia (NH_3), and VOCs for East Asia from the KORUS v2 emissions inventory Woo *et al*. (2012), biomass burning emissions from

the Global Fire Emissions Database 4 (GFED4) (van der Werf *et al.*, 2010), and on-line biogenic emissions calculated by the Model of Emissions of Gases and Aerosols from Nature (MEGAN) v2.1 (Guenther *et al.*, 2012).

Table 2.1. Default gas phase reactions of aromatic chemistry in GEOS-Chem based on Henze *et al*. (2008).

Reactants	Products	Rate constant		
		A	B	C
BENZ + OH	1.000BRO2	2.33E–12	0	–193
TOLU + OH	1.000TRO2	1.81E–12	0	338
XYLE + OH	1.000XRO2	2.31E–11	0	0
BRO2 + HO2	1.000LBRO2H	1.40E–12	0	700
BRO2 + NO	1.000LBRO2N	2.60E–12	0	350
TRO2 + HO2	1.000LTRO2H	1.40E–12	0	700
TRO2 + NO	1.000LTRO2N	2.60E–12	0	350
XRO2 + HO2	1.000LXRO2H	1.40E–12	0	700
XRO2 + NO	1.000LXRO2N	2.60E–12	0	350

Table 2.2. Aromatic species and reaction intermediates added in the updated aromatic mechanism.

Species name	Description
CRES	Cresol
PHEN	Phenol
EPX	Epoxide from BENZ
DCB	Unsaturated dicarbonyls
TCO3	Unsaturated acyl peroxy radical
XO2	RO_2 from CRES, PHEN, EPX
XNO2	RO_2 containing nitro groups from CRES, PHEN

2.2. O_3 formation sensitivity to aromatic chemistry

2.2.1. Evaluation of simulated O_3, NO_x, and VOCs

Figure 2.1 and Figure 2.2 compare model performances from the base model (BASE) using default chemistry and the model (AROM) with updated aromatic chemistry. The BASE model significantly underestimates O_3 and NO_x, with normalized mean biases (NMB) of −26% and −40%, respectively, although no significant low biases are shown for reactive VOCs. The update of aromatic chemistry in the model substantially increases simulated O_3 concentrations, resulting in better agreements with observations relative to those from the BASE model. The increase in O_3 production mainly results from more rapid NO_x recycling driven by aromatic VOCs oxidation, especially by toluene and xylene, which show decreases in simulated concentrations with the update in the model. As a result, the pre-existing low bias of simulated NO_x becomes even larger in the AROM model. This is also associated with increased formation of organic nitrates and PAN, which are important NO_x reservoirs produced during the oxidation of VOCs (Figure 2.2). Despite the decrease in simulated NO_x concentrations, the chemistry update effectively converts NO_x to organic nitrates, resulting in better agreements with observations.

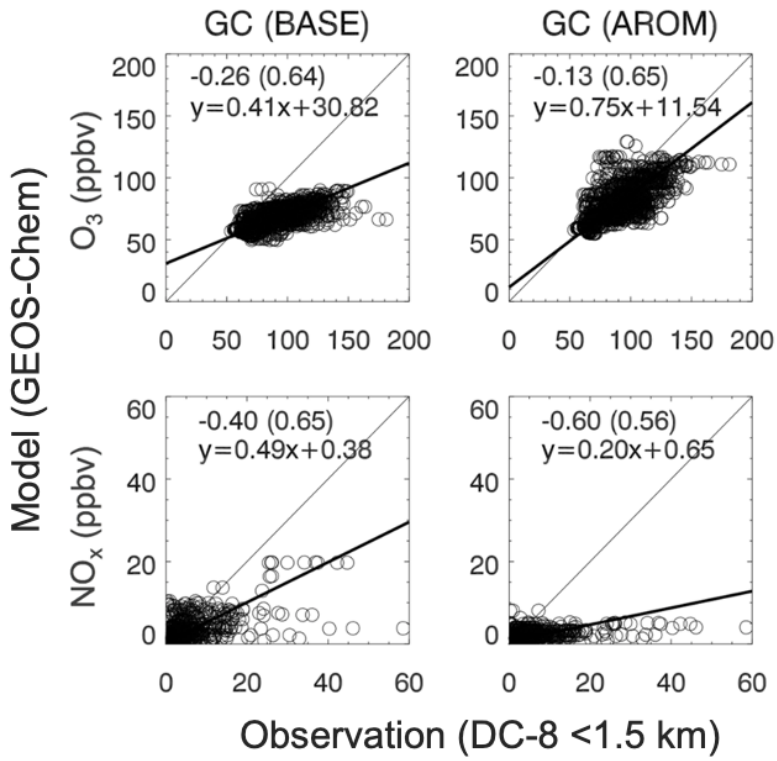

Figure 2.1. Scatterplot comparison of observed and simulated O_3 and NO_x in Korea during KORUS-AQ. The model performance statistics (NMB, R, regression slope) are denoted in upper-left corners.

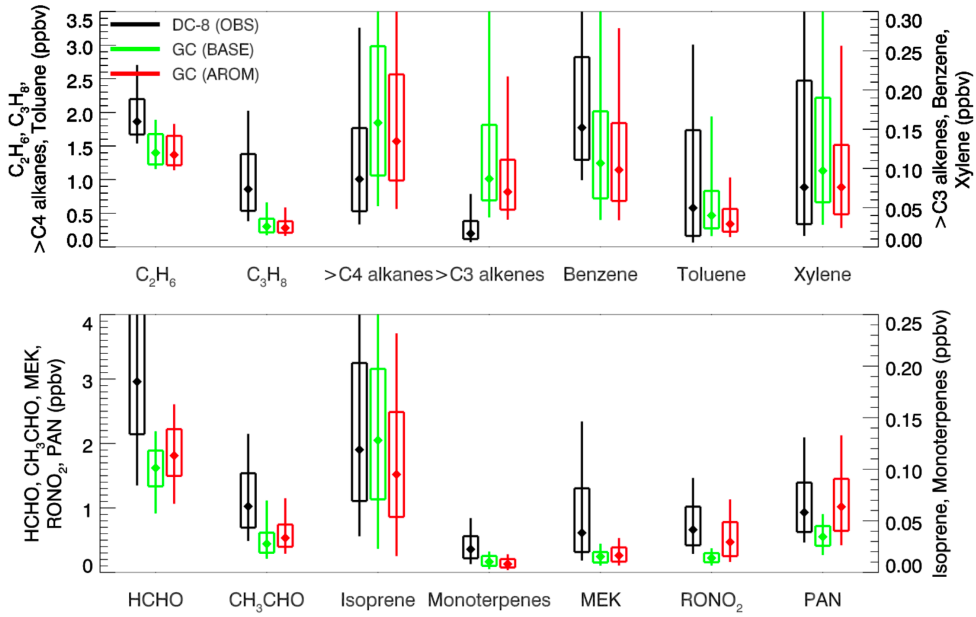

Figure 2.2. Comparison of observed and simulated organic nitrates, PAN, and speciated VOCs in Korea during KORUS-AQ.

2.2.2. Evaluation of simulated OPE

Figure 2.3 compares the campaign average O_3 formation, O_3 destruction, NO_x loss rates, and OPE from GEOS-Chem as calculated using Eq. (2.1−2.5) with results from the observation-constrained box model.

The O_3 formation rate, F_{O_3}, is calculated as the sum of the reaction rates of peroxy radicals and NO. Compared to the BASE simulation, updated aromatic chemistry increases both "HO_2+NO" and "RO_2+NO" terms but still underestimates F_{O_3} compared to the box model. NO_x underestimation appears to be the main cause of the low formation rates compared to the box model, as RO_2 is overestimated and HO_2 is underestimated in GEOS-Chem (not shown).

While the O_3 destruction rate, D_{O_3}, is also underestimated in GEOS-Chem, O_3 losses by the "O_3+HO_2" and "NO_2+OH" reactions show largest discrepancies between the two models (Figure 2.3b). An O_3 destruction increase by the "O_3+HO_2" reaction in the AROM model is associated with the increase in HO_2 mixing ratios. Despite the increase in the AROM model, the "O_3+HO_2" term is still smaller in GEOS-Chem than that of the box model, which can be explained by the underestimation of O_3 and HO_2 mixing ratios (not shown). The overestimation of >C3 alkenes (Figure 2.2) causes the overestimation of the "O_3+VOCs" term. The "NO_2+OH" contribution, which represents an O_3 loss by the reaction with NO, does not show a significant change from the BASE model to the AROM model. In both model runs, the

underestimation of NO_x shown in Figure 2.1 is the main contributor to the underestimation of O_3 loss rates by the "NO_2+OH" reaction relative to the box model result.

The difference between F_{O_3} and D_{O_3} is the net O_3 production rate, which is shown in Figure 2.3c. Updated aromatic chemistry increases the simulated net O_3 production and NO_x loss rates in GEOS-Chem by 37% and 22%. This explains the increase in O_3 and the decrease in NO_x mixing ratios shown in Figure 2.1. However, because NO_x is highly underestimated in GEOS-Chem, L_{NO_x} underestimation still exists.

NO_x underestimation may imply either the underestimation of emissions or model uncertainties in chemical, thermodynamic or physical processes such as NO_x recycling, reactive nitrogen (NO_y) partitioning or boundary layer mixing. Before evaluating NO_x emissions, I first examined the effect of mixing and dilution within the planetary boundary layer (PBL) on simulated daytime NO_x concentrations.

During the campaign, lidar observations at Seoul National University (SNU) were used to retrieve PBL heights and are used for the model evaluation in this study. Figure 2.4 compares simulated versus observed hourly PBL heights at SNU averaged for the campaign and large discrepancies of up to a factor 1.3 are found between the model and lidar-derived values during 13:00–15:00 LT. In order to test the effect of boundary layer mixing within the PBL in the model, I used average diurnal profiles of

the PBL to calculate hourly scale factors based on the discrepancy between the model and lidar observations at SNU. Although the hourly scale factors are based on model evaluation at only one grid box, same scale factors are applied to other model grid boxes for the rest of South Korea. The scaled PBL heights are lower in the daytime and higher in the nighttime compared to the PBL heights in the baseline model, reducing the gap between the model and lidar observations as shown in Figure 2.4. Constraining the daytime PBL heights based on the lidar-derived observations increases O_3 and its precursors mixing ratios in the model. Correspondingly, both the P_{O_3} and L_{NO_x} terms increase by ~10% and show better agreements with the box model results.

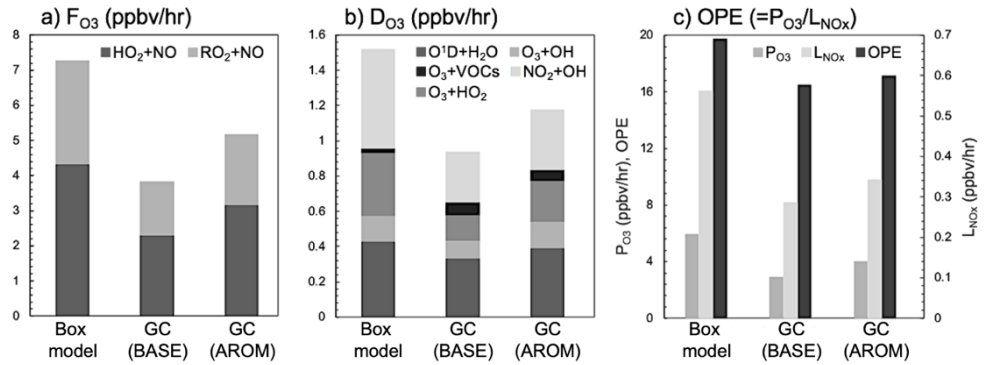

Figure 2.3. Comparison of simulated a) O_3 formation rate, b) O_3 destruction rate, and c) OPE in Korea during KORUS-AQ.

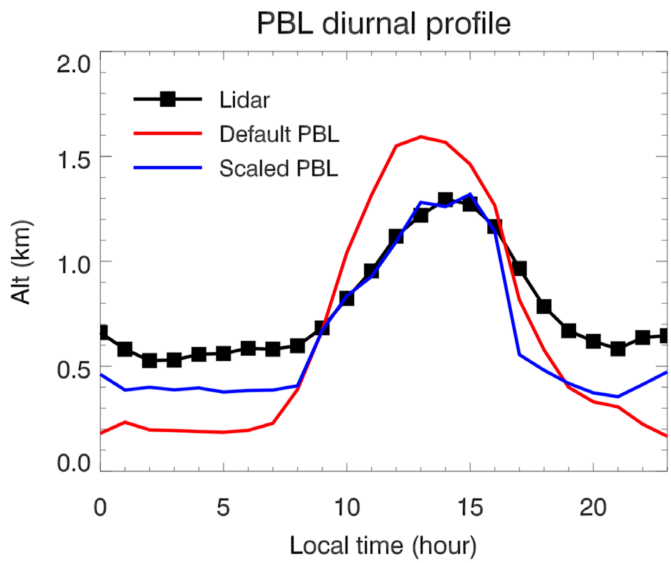

Figure 2.4. Diurnal profiles of observed (lidar) and simulated PBL heights at Seoul National University (37.46°N, 126.95°E) during KORUS-AQ.

2.3. Implications for O_3 precursor emissions

2.3.1. Evaluation of anthropogenic NO_x emissions in Korea

Based on the model underestimation of surface NO_x levels I increased NO_x emissions in South Korea by 50%. Figure 2.5 shows that when the emissions are increased, simulated NO_x mixing ratios are significantly enhanced and become much closer to the observations especially above 1 km. However, the 50% increase does not entirely reduce the gap between the model and observation during the entire campaign. Further analysis based on synoptic weather conditions shows that under the influence of stagnant conditions and blocking patterns when local emissions were the dominant sources of pollutants in Korea, the emissions increase in the model results in better agreement with observations.

Figure 2.6 shows the VOCs and NO_x dependency of instantaneous OPEs calculated in the box model and GEOS-Chem. VOCs include ethane, propane, large alkanes (>C4), large alkenes (>C3), benzene, toluene, xylene, isoprene, monoterpenes, methyl ethyl ketone (MEK), and acetaldehyde. In the observation-constrained box model, low OPE values are shown above the 10:1 line, representing VOC-limited O_3 production regimes. General characteristics of the observed OPE dependency on precursor concentrations also appear in GEOS-Chem. However, due to the underestimation of NO_x, GEOS-Chem results are slightly shifted to a NO_x-limited regime compared to the box model.

The simulated results with scaled PBL heights shown in Figure 2.6c−d show larger scatters compared to Figure 2.6b, elongating the location of the points diagonally, which is caused by the lower PBL height. Decreased PBL heights tend to decrease species mixing ratios in upper levels (~1.5 km) compared to the base PBL simulation. This results in decreases of NO_x and VOCs mixing ratios around 1.5 km, which correspond to the data points located in the lower left corners. The overall comparison of GEOS-Chem to the observation-constrained box model indicates that the model with scaled PBL heights and increased NO_x emissions (PBL+NO_x) shows the best performance in reproducing the observed O_3 production regimes in Korea.

Sensitivity simulations conducted in this study, which are consistent with the top-down analysis results from Goldberg *et al*. (2019), provided the rationale for the need for updates in the KORUSv2 inventory. The final version of the KORUS inventory, version 5, incorporated up-to-date national emissions inventories for Korea, China, and Japan. Also, Korean NO_x emissions were increased by 37%, as a result of updated on-road mobile emission factors (Crawford *et al.*, 2021). Figure 2.7 compares observed and simulated O_3, NO_x, toluene, and OA vertical profiles in the Seoul Metropolitan Area (SMA) during KORUS-AQ. Each row shows multi-model comparison using the first and final versions of the KORUS emissions. Model performances using the KORUSv5 inventory are improved for all species compared to the previous versions (Park *et al.*, 2021).

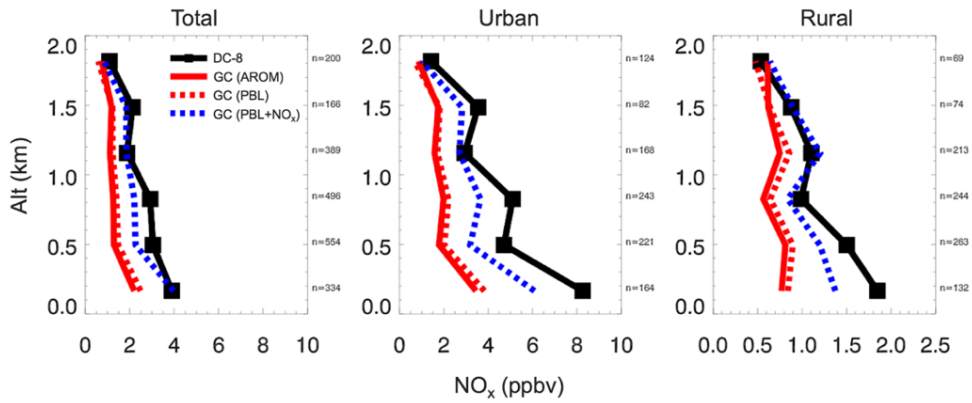

Figure 2.5. Mean vertical profiles of observed and simulated NO_x in Korea during KORUS-AQ.

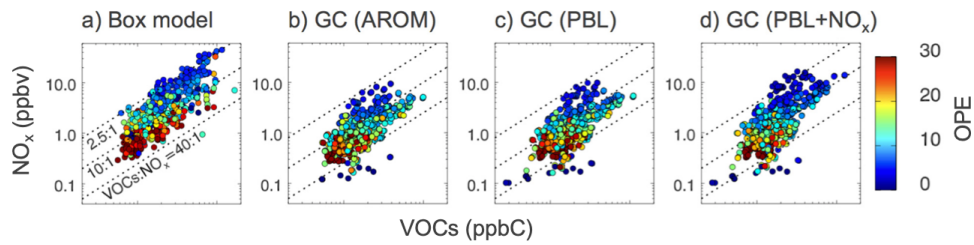

Figure 2.6. VOCs and NO_x dependence of instantaneous OPEs calculated from the box model and GEOS-Chem in Korea during KORUS-AQ.

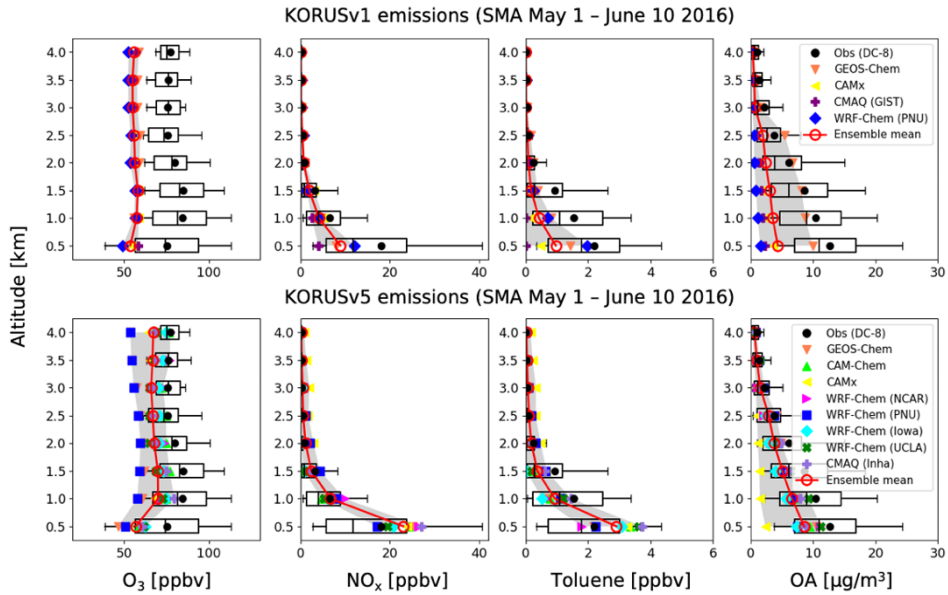

Figure 2.7. Multi-model intercomparison during KORUS-AQ using updated (KORUSv5) NO_x emissions.

2.3.2. Sensitivity of OPE to emission changes in Korea

The Korean government aimed to achieve a 30% reduction of domestic emissions by 2022 as part of the $PM_{2.5}$ concentrations reduction policy. However, this emission change may also have a profound impact on O_3 levels in Korea. To estimate the effect of regulation I conducted sensitivity simulations and investigated the change in O_3 and the OPE with respect to emissions control in the future. Using the best-performing model (PBL+NO_x) as the base run, model sensitivity to reduction in NO_x and anthropogenic VOCs emissions over Korea is examined.

Figure 2.8 shows the spatial distributions of simulated ground level OPEs during May 2016. Typical features of the OPE such as high in clean regions and low in polluted regions are well captured. In the base run, maximum OPE of ~20 along the mountain range located in the middle is noticeable, where biogenic VOCs emissions are dominant, and minimum values in high NO_x regions such as the SMA. In both the sensitivity runs the reduction in emissions increases the OPE throughout the country. When only NO_x emissions are controlled, the OPE reaches up to 30 in rural regions, indicating that these NO_x-limited regions become much more efficient in producing O_3 with the same amount of NO_x. With NO_x and VOCs emissions controlled together, the OPE increase is less prominent, showing a maximum of ~25.

Figure 2.9 shows O_3 changes as a response to the emissions control. In

rural regions where NO_x plays the major role in O_3 production, O_3 decreases and the NO_x lifetime increases due to less oxidation by OH (i.e., decrease in NO_x loss). In urban (e.g., Seoul, Busan) and industrial areas (e.g., Daesan, Pohang, Ulsan, Yeosu) which are under VOC-limited conditions, O_3 increases (~6 ppbv) and NO_x lifetimes show noticeable decreases as a result of NO_x reductions. With concurrent VOCs reductions, although there are some signals of O_3 increase in industrial areas the magnitudes are significantly smaller than those without VOCs reductions, and O_3 decreases are shown in major metropolitan areas. These simulations clearly show that 30% decrease in NO_x emissions does not directly decrease O_3 mixing ratios by 30% because of the nonlinear chemistry, and that VOCs reductions must be carried out together for the abatement of ground level O_3.

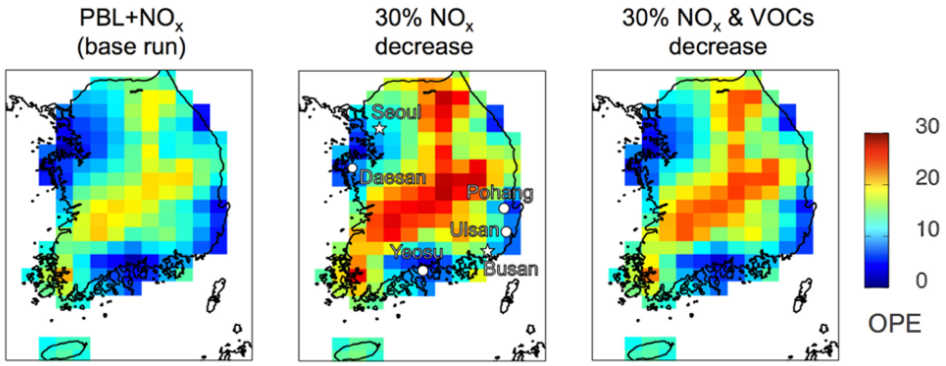

Figure 2.8. Spatial distributions of simulated OPE at surface level and responses to emission change during May 2016.

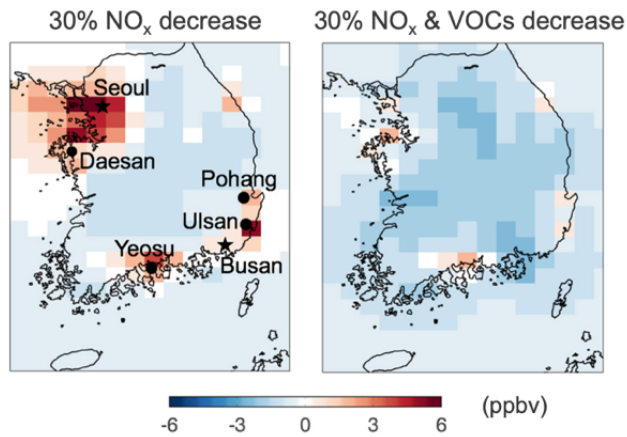

Figure 2.9. Spatial distributions of simulated O_3 changes (modified emissions minus base) as responses to emission change during May 2016.

2.4. Summary and implications

Model evaluation between simulated OPE using a 3-D CTM and an observation-constrained 0-D box model showed that aromatic chemistry can increase the average net O_3 production in Korea by 37% during the springtime. The implementation of a detailed aromatic chemistry scheme in the model increased simulated O_3 levels by 13%, driven by increased NO_x recycling. These results are consistent with a global study which found increased radical recycling and O_3 destruction, resulting in significant increases in annual mean O_3 levels, especially in East Asia, with the inclusion of aromatic oxidation in GEOS-Chem (Bates *et al.*, 2021).

Sensitivity tests with the updated aromatic chemistry scheme showed that a 30% decrease in anthropogenic emissions increases the OPE throughout the country, making rural regions ~2 times more efficient in producing O_3. However, without the VOCs reduction, the NO_x reduction alone can result in significant increases in O_3 levels in urban and industrial regions. This implies the importance of concurrent emission reductions for both NO_x and VOCs in order to effectively reduce O_3 levels in Korea.

Chapter 2 emphasizes the essential role of gas phase aromatic chemistry in producing secondary pollutants in Korea regarding their relative abundance and reactivities. In the following chapter, I will examine the role of aromatics as a precursor of particle formation in urban environments in Korea.

Chapter 3. Chemical formation and loss processes of organic aerosols (OA)

Along with O_3, complicated atmospheric processes of precursor species determine the chemical composition of PM. Observational studies show that OA represents a large fraction (20–90%) of total PM_1 concentrations globally (Zhang *et al.*, 2007; de Gouw and Jimenez, 2009; Zhou *et al.*, 2020). A significant amount of OA mass has also been reported in East Asian mega-cities. For example, in Seoul, a densely populated megacity with a population of ~10 million, OA comprises roughly 40% of total non-refractory PM_1 mass concentrations during late spring (Jordan *et al.*, 2020; Crawford *et al.*, 2021). In this chapter, I investigated the chemical formation and loss processes of OA to understand the regional and seasonal characteristics of observed OA in Seoul.

Organic species are often directly emitted in the particle phase from combustion sources, both anthropogenically and naturally, which are known as POA (Zhang *et al.*, 2007; Jimenez *et al.*, 2009). On the other hand, SOA can be formed from the oxidation of precursor gases, called parent hydrocarbons or VOCs, and through the gas-particle partitioning process of these oxygenated organic compounds (de Gouw and Jimenez, 2009; Hallquist *et al.*, 2009). Compared to inorganic species that comprise PM, such as sulfate (SO_4^{2-}), nitrate (NO_3^-), and ammonium (NH_4^+) aerosols, scientific understanding of the atmospheric formation and removal processes of OA,

especially the atmospheric processing of SOA in urban environments, is still highly uncertain (Hayes *et al.*, 2015). Not only are direct emissions of POA difficult to estimate, but also the sources, atmospheric fates, characterization of precursor species, and the volatility distribution of SOA remain as a large uncertainty.

Modeling SOA requires both accuracy and simplicity so that the schemes reproduce important characteristics of the complex processes that lie behind SOA formation, and at the same time, they need to be computationally efficient. One of the most traditional SOA modeling schemes is the "two-product approach", which uses two SOA surrogates that partition at equilibrium based on SOA yields from chamber experiments (Odum *et al.*, 1996). Later, a new approach was introduced to represent continuous oxidation of semivolatile compounds, also known as chemical aging, with the volatility distribution of OA. Donahue *et al*. (2006) and Stanier *et al*. (2008) developed the "volatility basis set (VBS) approach", which divides the wide volatility range into several bins that categorize organic compounds by their volatilities, and when subject to aging, their volatilities would change.

Although recent studies show enhancement in simulated SOA mass, showing improved results compared to the large model-observation discrepancies that have been reported previously, study regions and model resolutions have been limited to a global scale (Jo *et al.*, 2013; Hodzic *et al.*, 2016; Pai *et al.*, 2020). In this chapter, I examined the characteristics of OA

formation in an urban environment in Korea, on a finer scale, using airborne and ground observation data along with GEOS-Chem. I compared four SOA schemes, including a simplified approach and three different treatments using the VBS method, and evaluated model performance in Seoul during different seasons in 2016 through 2018. The main objective of this study is to suggest the most suitable approach in representing the observed atmospheric conditions for OA in Seoul.

3.1. Method

3.1.1. Model configuration

I used GEOS-Chem v12.0.0 and its nested configuration to simulate OA (Bey *et al.*, 2001) in East Asia during two different periods, spring-summer 2016 and fall-winter 2017/2018. Meteorological input (GEOS-FP assimilated meteorology), horizontal/vertical resolutions, and simulation domains of the global and nested simulations are identical as the description in Section 2.1.2.

For emission inputs I used monthly anthropogenic emissions of CO, NO_x, SO_2, NH_3, VOCs, black carbon (BC), and primary organic carbon (POC) for East Asia from the KORUS v5 emissions inventory (Woo *et al.*, 2020), biomass burning emissions from GFED4 (van der Werf *et al*., 2010), and on-line biogenic emissions calculated by MEGAN v2.1 (Guenther *et al*., 2012). Although anthropogenic emissions from the KORUS v5 inventory are based on 2015–2016 estimates, I did not apply additional scaling or projections for 2017/2018 simulations as previous studies and statistics showed that anthropogenic emissions in Korea and China did not show significant annual trends from 2016 through 2018 (Zheng *et al.*, 2018; NIER, 2020).

GEOS-Chem simulates POC and SOA separately and defines tracers according to their hydrophilicity for POC, and volatility for SOA. The model simulates two POC tracers, “OCPO” for hydrophobic POC and “OCPI” for hydrophilic POC, assuming that 50% of POC is emitted from combustion sources as OCPO, which is converted to OCPI with a lifetime of 1.15 days

(Cooke *et al.*, 1999; Park *et al.*, 2003). For conversion of POC to POA, I multiplied the simulated POC concentrations by an organic aerosol to organic carbon ratio (OA/OC) of 1.3 based on observation-based studies (Xing *et al.*, 2013; Huang *et al.*, 2017; Kim *et al.*, 2017) in East Asia. The model assumes an OA/OC ratio of 2.1 to calculate SOA partitioning and simulates SOA tracers as organic matter with molecular weights of 150–250 g mol^{-1}.

Section 3.2 compares four different SOA schemes, including the two standard SOA options in GEOS-Chem, the "Complex" (Pye *et al.*, 2010) and "Simple" (Hodzic and Jimenez, 2011) schemes, and two additional schemes introduced by Hodzic *et al*. (2016) and Jo *et al*. (2013), hereafter referred as the "Hodzic" and "Jo" schemes. Brief explanations on the main features and updates in each scheme are summarized in Table 3.1. All schemes except the Simple scheme use the VBS approach, which allocate oxygenated organic compounds that are formed by the reactions between oxidants and parent hydrocarbons such as isoprene, terpenes (monoterpenes, sesquiterpenes), aromatics (benzene, toluene, xylene), and semi/intermediate volatile organic compounds (S/IVOCs), into several bins according to their saturation concentrations (C*). Anthropogenic and biomass burning emissions of S/IVOCs are estimated by scaling 50% of POA and 20% of NMVOCs emissions (Jathar *et al.*, 2014).

Table 3.1. Comparison of the four SOA schemes used in this study. Aromatics indicate benzene, toluene, and xylene.

Scheme	SOA precursors	VBS bins	SOA aging	SOA yield	Additional description
Complex	Isoprene, terpenes, aromatics	Four bins (C* = 0.1–100)	Only within VBS bins	Ng *et al*. (2007), Shilling *et al*. (2009), Zhang *et al*. (2006)	Updated isoprene chemistry and SOA formation
Simple	SOAP (scaled from isoprene, terpenes, CO emissions)	N/A	N/A	100% (irreversible formation)	SOAP 100% converted to SOAS with a lifetime of 1 day
Hodzic	Isoprene, terpenes, aromatics, S/IVOCs	Six bins (C* = 0.01–1000)	Only within VBS bins	Hodzic *et al*. (2016), Zhang *et al*. (2014)	Stronger production (wall-corrected yields) and faster removal (updated H^{eff}, photolysis, oxidation by O_3)
Jo	Isoprene, terpenes, aromatics, S/IVOCs	Five bins (C* = 0.1–1000)	Within VBS bins + functionalization	Farina *et al*. (2010)	Chemical aging (functionalization) of SOA from aromatics and S/IVOCs

3.1.2. Observations

I used airborne and surface observations of OA mass concentrations measured using the high-resolution time-of-flight aerosol mass spectrometer (HR-ToF-AMS, hereafter denoted as "AMS") (DeCarlo *et al.*, 2006), and surface observations of carbonaceous aerosols, i.e., organic carbon (OC) and elemental carbon (EC), measured using the OCEC carbon aerosol analyzer (Sunset Laboratory Inc.) at Seoul for model evaluation during spring-summer 2016 and fall-winter 2017/2018. Supporting observations of VOCs, CO, O_3, NO_x, and NO_y (= NO_x + HNO_3 + NO_3^- + PAN + $RONO_2$ + etc.) are also used for analysis.

During the KORUS-AQ (spring 2016) campaign, airborne (DC-8) and surface (KIST) AMS observations of OA mass concentrations were measured and further analyzed by Nault *et al*. (2018) and Kim *et al.* (2018), respectively, providing detailed information on the composition of OA using the positive matrix factorization (PMF) analysis (Ulbrich *et al.*, 2009). Nault *et al.* (2018) apportioned DC-8 observations of OA into six factors, then recombined them to three organic components: hydrocarbon-like OA (HOA), less-oxidized oxygenated OA (LO-OOA), and more-oxidized oxygenated OA (MO-OOA). In this study, I define POA as HOA, and SOA as the sum of LO-OOA and MO-OOA. Kim *et al*. (2018) applied PMF analysis to ground observations of OA at the KIST site and also identified four organic components: hydrocarbon-like OA (HOA), cooking-influenced OA (COA), low-volatility

oxygenated OA (LV-OOA), and semi-volatile oxygenated OA (SV-OOA). For the KIST data, I define POA as the sum of HOA and COA, and SOA as the sum of LV-OOA and SV-OOA.

Ground observations of OC and EC are used for analysis for the rest of the analysis periods. The ground site in Seoul is located in Bulkwang (37.61°N, 126.93°E). The semi-continuous OCEC analyzer (Sunset Laboratory Inc.) was used to observe hourly mass concentrations of carbonaceous aerosols at the Bulkwang site.

As PMF analysis is not applicable to the OC observations collected by the OCEC analyzer, total OC observations do not provide any information on the sources of OC. Therefore, I employed the EC tracer method (Turpin and Huntzicker, 1995) to estimate the primary and secondary fractions in the observed total OC. Assuming that POC and EC are co-emitted from combustion sources, the primary OC to EC ratio, $(OC/EC)_{primary}$, is estimated by locating where OC is strongly correlated with EC and is less associated with non-combustion sources. POC and SOC concentrations can then be calculated using Eq. (3.1–3.2).

Eq. (3.1) $POC = (OC/EC)_{primary} \times EC + OC_{non-combustion}$

Eq. (3.2) $SOC = OC - POC$

In this study, I used Deming regression analysis to determine the slope and intercept that best represent the relationship between ambient OC and EC datasets that show high correlation (Pio *et al.*, 2011; Jeon *et al.*, 2015; Wu and

Yu, 2018). Table 3.2 compares the regression slope, i.e., $(OC/EC)_{primary}$, used for each analysis period and the resulting monthly mean SOA mass fractions (%), which is defined as SOA/(SOA+POA). A POA/POC value of 1.3 and OA/OC values of 1.8 (spring-summer) and 1.6 (fall-winter) are applied for different seasons to convert the estimated POC and SOC to POA and SOA.

The estimated secondary portions of the observed OA mass concentrations at the Bulkwang and Olympic Park sites during KORUS-AQ are 62% and 53%, respectively. PMF results at the KIST site for the same period showed that 61% of observed OA mass was related to secondary formation. The secondary fraction may differ on a local scale, on whether the measurement site is affected by heavy traffic, residential emissions, biogenic emissions, etc. (Robinson *et al.*, 2007). All three sites are located near busy roads surrounded by large residential areas. The EC tracer method shows consistent results with the PMF analysis results for surface air in Seoul regarding the various local environments surrounding each measurement site.

Table 3.2. $(OC/EC)_{primary}$ values determined by Deming regression between surface OC and EC measurements used in the EC tracer method and resulting monthly mean SOA mass fractions (%) for each period.

Deming fit	May 2016	July 2016	October 2017	December 2017	February 2018
$(OC/EC)_{primary}$	0.78 ± 0.01	1.08 ± 0.01	2.76 ± 0.10	3.20 ± 0.01	3.43 ± 0.05
SOA fraction (%)	76 ± 2	81 ± 2	41 ± 3	37 ± 2	56 ± 2

3.2. Evaluation of SOA simulations for Seoul, Korea

3.2.1. Model evaluation during KORUS-AQ

Figure 3.1 compares daily mean timeseries of observed and simulated total OA (= POA + SOA) concentrations using different SOA schemes at Seoul during 1 May–10 June 2016. Surface values were averaged at three ground sites (Bulkwang, KIST, Olympic Park) and compared to the closest model grid box values. AMS observations of POA and SOA, characterized using PMF analysis, in the boundary layer (< 1.5 km) along the DC-8 flight track over Seoul (37.4–37.6°N, 127–12 7.2°E) are compared with simulated OA concentrations, which were sampled coherently in time and space. Mean vertical profiles within the SMA from the ground to 5 km are also shown for comparison.

Observed total OA concentrations at the ground sites and onboard the DC-8 show similar temporal variations, with a distinct peak during 19–24 May, caused by a considerable enhancement of SOA. PMF results showed that SOA observed at KIST and onboard the DC-8 during this period were more likely to be aged and less volatile, indicating that photochemistry and aging processes associated with long-range transport enhanced SOA formation (Kim *et al*., 2018; Nault *et al*., 2018).

The ensemble model, representing the arithmetic mean of the four schemes, shows a 6% underestimation compared to ground observations of total OA, with NMB from individual schemes ranging from −42% to 35%

(Figure 3.1a). Correlation coefficients (R) between the simulations and observation lie within 0.24 to 0.58. Overall, the Jo scheme simulates the highest OA concentrations followed by the Simple scheme, which lies between the amounts simulated by the Hodzic and Jo schemes. The Hodzic and Jo schemes better represent daily variations of observed OA ($R \geq 0.42$) compared to the Simple scheme ($R = 0.24$).

All schemes except for the Jo scheme underestimate airborne observations of total OA in the boundary layer, with correlation coefficients ranging from 0.37 to 0.59 (Figure 3.1b). The ensemble model underestimates OA in the Seoul boundary layer by 27%, with a temporal correlation coefficient of 0.51. Underestimation is consistently shown in the Complex scheme (NMB = −43% and −55% in surface air and the boundary layer, respectively), indicating that additional sources and updated yield parameters are necessary for reproducing observed OA concentrations in Seoul.

In order to investigate the cause of the model-observation discrepancies, I also compared observed and simulated SOA precursors for KORUS-AQ. Figure 3.2 shows the daily mean timeseries of gaseous species at the Bulkwang, Guui, and Olympic Park ground sites and in the boundary layer along the DC-8 flight track over Seoul.

CO, which is used as a tracer for estimating fossil fuel and biomass burning emissions of SOAP in the Simple scheme, is consistently underestimated compared to both ground and airborne observations. This

issue was addressed in several studies as an uncertainty in the KORUS v5 bottom-up emissions inventory (Gaubert *et al.*, 2020; Park *et al.*, 2021). Among the significant biogenic species, isoprene is overestimated at the surface (NMB = 45%) and in the boundary layer (NMB = 9%). Simulated aromatics (= benzene + toluene + xylene) are also overestimated compared to ground observations but generally follow the observed daily variations. In contrast, the model shows an underestimation and poor correlation compared to airborne observations. This discrepancy may imply model uncertainties associated with boundary layer mixing and gas-phase chemistry, requiring additional validation sensitivity tests.

Daily variations of precursor species were likely to be highly influenced by synoptic patterns (Peterson *et al.*, 2019). Therefore, in the following paragraphs I will evaluate model performance regarding the effect of meteorological conditions on SOA and its precursors. Four different synoptic periods are indicated in colored shadings in Figure 3.1 and Figure 3.2.

Dynamic weather period (1−16 May)

The first two weeks of May were characterized as a dynamic weather period with frequent precipitation and relatively strong surface wind. Rain events and strong winds are well represented in the model compared to surface observations. However, simulated diurnal variations of aromatic species during this period show sharp nighttime through early morning peaks caused by too low nighttime boundary layer heights in the model, which was

pointed out in Section 2.2.2 (Figure 2.4), resulting in overestimations of daily mean values.

High organic period (17−24 May)

This period was influenced by stagnation and large-scale subsidence (Peterson *et al*., 2019), resulting in the weaker surface wind with warm and dry conditions. All schemes fail to simulate SOA enhancement during the high organic period, although simulated precursor VOCs concentrations do not show any negative biases from observations. While the model simulates larger cloud fractions than observations, insufficient photochemistry or missing sources from transboundary transport may have contributed to the underestimation of SOA formation.

High inorganic period (25−31 May)

Seoul experienced extreme $PM_{2.5}$ pollution, frequently exceeding the Korean 24-hour standard of 35 μg m^{-3}, and bad visibility during 25–31 May (Jordan *et al.*, 2020) due to a mixture of local emissions and transport of pollutants from China caused by predominant westerlies and frontal passages. Simulated fine PM, CO, and aromatic VOCs tend to follow the observed fluctuations, showing that the model successfully captures the eastward transport of anthropogenic pollutants. However, high precursor concentrations cause the overestimation of SOA in the Simple and Jo schemes, as the SOA timeseries from both schemes generally follow the timeseries characteristics of their main precursor species: CO and aromatics.

Blocking pattern period (1−7 June)

During 1–7 June, a blocking pattern that consisted of a high-pressure system located north of a low, caused stagnant conditions and inhibited the long-range transport of pollutants to the Korean peninsula, which resulted in accumulation of local pollutants. The model shows considerable overestimations of aromatic VOCs and secondary inorganic aerosols (not shown) caused by peaks during 21:00–06:00 LT, mainly due to the shallow nighttime boundary layer in the model, similar to that during the dynamic weather period. Simulated diurnal profiles of aromatics and SOA during this period show similar variations, indicating that the shallow boundary layer and overestimation of precursor VOCs are likely the main cause of SOA overestimation.

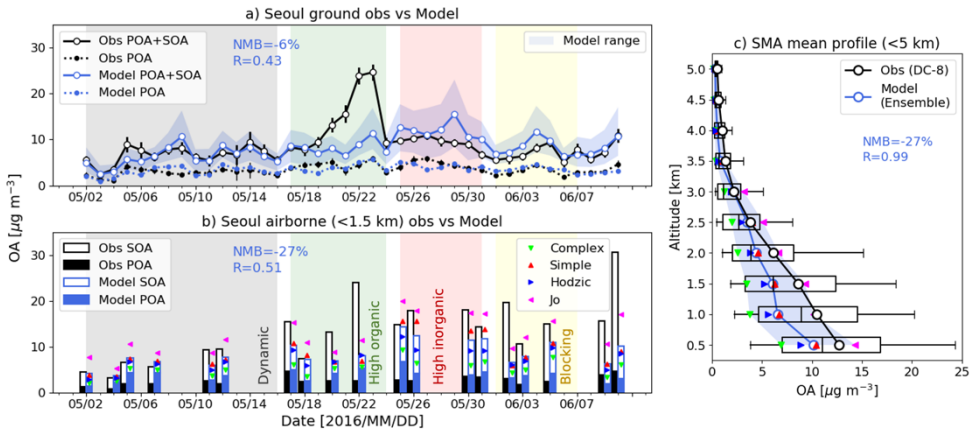

Figure 3.1. Comparison of observed and simulated daily mean a) surface and b) airborne (<1.5 km) OA, POA, and SOA concentrations at Seoul, and c) OA vertical profiles in the SMA during KORUS-AQ 2016. Observations and the ensemble model are indicated in black and blue bars and circles, and individual models are shown in different colors. The colored shadings indicate the synoptic periods discussed in the text.

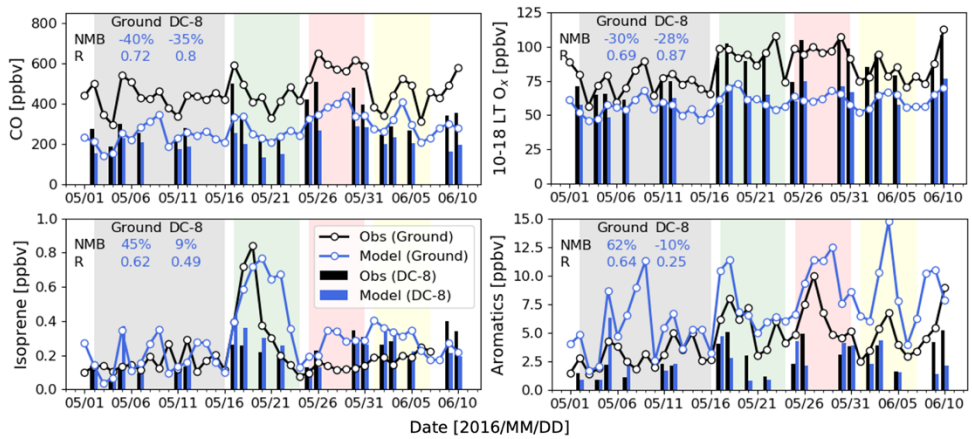

Figure 3.2. Comparison of observed and simulated daily mean CO, daytime (10:00−18:00 local time) O_x (= O_3 + NO_2), and SOA precursors including aromatic VOCs (= benzene + toluene + xylenes) and isoprene at Seoul during KORUS-AQ 2016. Solid lines and bars indicate surface timeseries and average values of each research flight onboard the DC-8, respectively. The colored shadings indicate the synoptic periods discussed in the text.

Figure 3.3 compares the observed and simulated dilution-corrected SOA/ΔCO enhancement ratios during KORUS-AQ, which show the photochemical evolution of SOA and degree of atmospheric aging. To account for the dilution of SOA with background air during its formation, I used the dilution-corrected CO ($\Delta CO = CO_{ambient} - CO_{background}$) and calculated photochemical age incorporating the NO_x/NO_y clock (Kleinman *et al.*, 2008).

To represent the observed $CO_{background}$ in Korea, I used a value of 200 ppbv, which Nault *et al.* (2018) identified using back-trajectory analysis during KORUS-AQ. To identify the simulated $CO_{background}$ value, I conducted a tagged CO simulation for the KORUS-AQ period using identical meteorology and emissions that I used for model evaluation. The resulting tagged CO simulation showed that the simulated average background CO in the boundary layer is 127 ppbv. I did not account for the background value of SOA, assuming that the majority of SOA in the SMA is formed on a local scale based on observational analysis (Nault *et al.,* 2018).

Observed airborne SOA/ΔCO ratio gradually increases with photochemical age, with a sharp gradient between 5−15 hours. The observed tendency is also dependent on the flight altitude, where both the SOA/ΔCO ratio and photochemical age increase with altitude (not shown). Simulated SOA/ΔCO ratios in the boundary layer are underestimated compared to airborne observations, regardless of SOA schemes. This is consistent with

model evaluation results in the previous paragraphs, where all models underestimated the observed vertical profile of OA mass concentrations. The Jo scheme best represents the observed rapid formation between 5−8 hours among the four schemes. A noticeable increase in the aromatic SOA portion in the Jo scheme results from the additional functionalization process. However, while observed SOA production continues to increase between 20−24 hours, simulated SOA production peaks before 20 hours and either remains flat or declines afterward, explaining the cause of SOA underestimation during 17−22 May. Overall comparison of observed and simulated enhancement ratios suggests that most schemes underpredict SOA aging in the boundary layer.

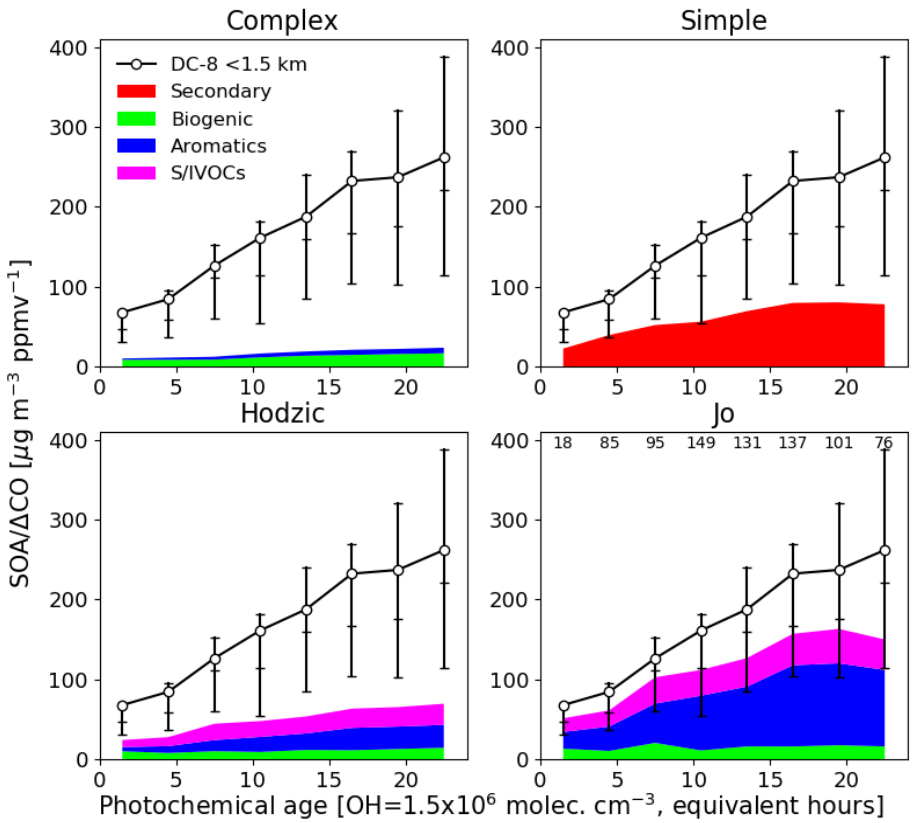

Figure 3.3. Observed and simulated mean SOA/ΔCO ratios versus photochemical age calculated along the DC-8 flight tracks in the SMA below 1.5 km during KORUS-AQ 2016. The number of data points used for binning is denoted in the lower-right (Jo) panel. Vertical bars indicate the interquartile range and the median of observed values.

3.2.2. Seasonal characteristics of OA in surface air

In addition to the KORUS-AQ period evaluation, here I evaluated simulated results during summer 2016 and fall-winter season of 2017/2018 using surface OCEC measurements and the EC tracer method at the Bulkwang site in Seoul.

Spring-summer season

Figure 3.4a–c compare observed and simulated mean POA and SOA concentrations in the boundary layer in the SMA and at ground sites in Seoul during May and July 2016. PMF results using airborne (DC-8) AMS measurements show a large secondary fraction (88%) and a relatively small primary fraction. Observed surface SOA during spring-summer makes up 66% of total OA mass in Seoul, resulting in a more significant primary fraction than the airborne data. PMF analysis of surface OA implies that this discrepancy may be due to the influence of cooking-related primary organic emissions, resolved as the COA factor, which is more likely to be captured in surface air (Kim *et al*., 2018). Therefore, the POA fraction in DC-8 observations can be interpreted as a lower limit in the SMA boundary layer.

Simulated POA concentrations are consistently overestimated compared to observations during the spring and summer seasons, implying either an overestimation of POA emissions or that the semivolatility of POA should be considered in models.

As discussed in previous sections, the inclusion of S/IVOCs and

chemical aging, i.e., functionalization, of SOA can improve the skill of the OA simulation. However, among the SOA schemes that incorporate S/IVOCs as SOA precursors, the Hodzic scheme often underestimates observed surface SOA concentrations. The Jo scheme tends to show overestimation due to the significant enhancement of the aromatic SOA portion. Therefore, I further examined the effect of chemical aging on simulated OA by conducting a sensitivity simulation combining the two schemes.

Figure 3.4a–b compare results of PMF analyses and model performance during the KORUS-AQ period with the inclusion of chemical aging using an aging constant of 4×10^{-11} cm^3 $molecule^{-1}$ s^{-1} to the Hodzic scheme. Semivolatile SOA (SV-SOA) and low-volatility SOA (LV-SOA) represent the oxidized components (OOA) of observed OA. SV-SOA refers to SOA with $C^* \geq 1$ and the rest are defined as LV-SOA in the model. Chemical aging of aromatic SOA increases simulated total SOA concentrations by 14–22% in the SMA. I find that the simulated mass of low-volatility ($C^* \leq 0.1$) SOA increases by 27–40%, while the semivolatile ($C^* \geq 1$) portion remains unaltered. Although all models, including the aging Hodzic and Jo schemes, underestimate SOA formation in higher altitudes within the boundary layer, the aging Hodzic scheme shows the best performance in reproducing observed SOA in surface air.

Fall-winter season

Figure 3.4d compares observed and simulated mean surface POA and

SOA concentrations at Seoul during October, December 2017, and February 2018. Estimated POA concentrations using OC and EC observations are significantly higher than those during spring and summer, reflecting the observed seasonal variation of EC caused by increased residential or open heating and prevailing westerlies carrying pollutants from upwind regions (Park *et al.*, 2015). However, the models tend to underestimate observed POA concentrations and show lower POA concentrations during the fall-winter period compared to the spring-summer period.

Most POA emissions in the KORUS v5 inventory are from mobile on-road transportation in Seoul. According to the Korea Expressway Cooperation (http://www.ex.co.kr) and Seoul Transport Operation and Information Service (https://topis.seoul.go.kr/), traffic volumes in Seoul and nearby expressways tend to increase with temperature and decrease with bad weather such as rain or snow, resulting in higher traffic during spring and summer than in winter. Therefore, the seasonal variation of traffic emissions is imposed in total anthropogenic POA emissions, which results in low simulated POA concentrations during the fall-winter period. The mismatch between the seasonalities of POA emissions from KORUS v5 and observed carbonaceous aerosols calls for revision of bottom-up emissions.

Observed SOA fractions at Seoul are smaller than 50%, and OA concentrations show a relatively weak correlation with photochemistry during the fall-winter period (not shown). The Simple and Jo schemes

overestimate simulated SOA concentrations and SOA fractions. Although underestimation of CO is more evident during this period (NMB = −56 to −66%) compared to spring-summer (NMB = −16 to −40%), the Simple scheme simulates excess SOA, indicating that either the SOAP emissions scaled from CO emissions are too large or the assumed lifetime (1 day) of SOAP may be too short causing the rapid formation of SOA in the fall-winter seasons in Seoul. On the other hand, simulated aromatic VOCs are generally overestimated in the model (not shown), resulting in an overestimation of SOA simulated from the Jo scheme.

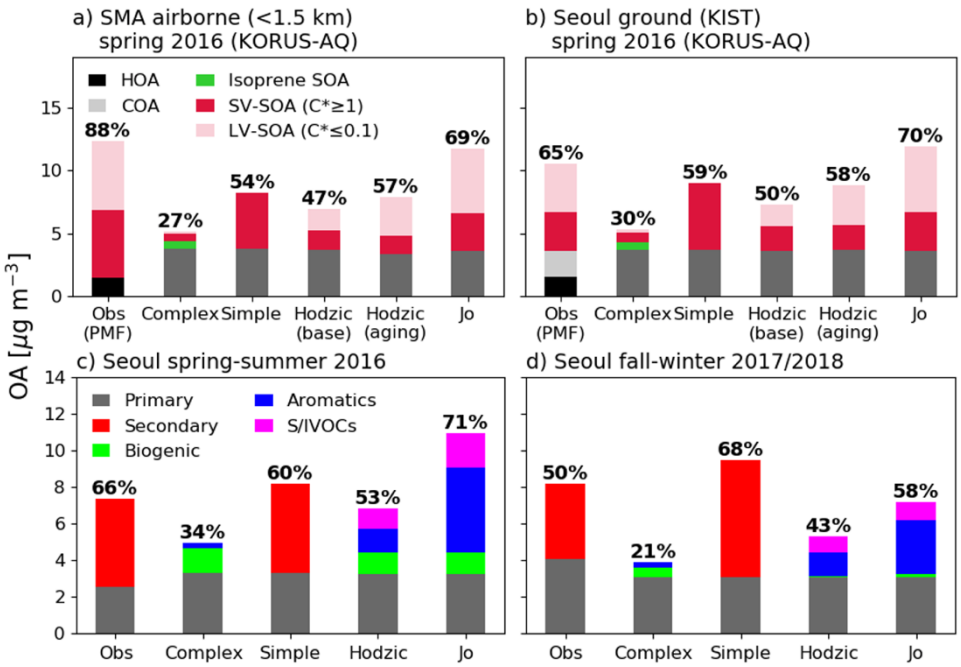

Figure 3.4. Comparison of observed and simulated mean OA concentrations a–b) in the SMA boundary layer and at the KIST ground site during KORUS-AQ and c–d) at Seoul ground sites during different seasons. Observed and simulated SOA fractions (%) are denoted above each bar. In panels a–b) PMF-resolved OA components during KORUS-AQ are compared with simulated results.

3.3. Summary and discussion

In Chapter 3, I used GEOS-Chem to simulate OA in Seoul using four different SOA schemes (Complex, Simple, Hodzic, Jo) during spring-summer 2016 and fall-winter 2017/2018. During the spring-summer seasons, the Jo scheme simulated the highest SOA concentrations, owing to chemical aging processes, followed by the Simple and Hodzic schemes. The Complex scheme underestimated observed SOA concentrations compared to the Hodzic and Jo schemes, regardless of seasons, indicating the necessity of additional SOA precursors. The Simple scheme simulated the largest amounts during fall-winter, followed by the Jo and Hodzic schemes.

To conclude, for better model representation of SOA formation in urban environments such as in Seoul, I recommend the inclusion of additional S/IVOCs precursors and chemical aging processes of SOA. However, as SVOCs and IVOCs are not included in traditional inventories, it should be noted that uncertainties remain on the treatment of S/IVOCs emissions. For computational efficiency, the Simple SOA scheme is a good alternative but can lead to biases associated with bottom-up CO emissions depending on the study region. For example, in Beijing, while simulated CO concentrations were underestimated, the Simple scheme significantly overestimated the SOA fraction compared to surface observations (74% versus 45%) during fall-winter 2017/2018.

In terms of reproducing the photochemical characteristics of observed

surface SOA in Seoul, the aging Hodzic scheme (Hodzic VBS + SOA aging) showed good performance. Based on these results, I applied the aging Hodzic scheme to simulate air quality in Korea for my analysis in the following chapter. However, the SOA yields used in the Hodzic VBS framework were generated using the Statistical Oxidation Model (SOM), which can account for the chemical aging of SOA (Hodzic *et al*., 2016). Therefore, the usage of the SOM-derived yields and the implementation of additional SOA aging processes in the model may result in an overprediction of chemical aging. A recent study derived VBS parameters of SOA in Seoul by coupling thermodenuders (TD) and ambient AMS observations (TD-AMS) (Kang *et al.*, 2022). Unlike chamber experiments, the TD-AMS method utilizes ambient measurements, and therefore does not account for SOA aging, which may be applicable to the explicit SOA aging schemes in the model.

Chapter 4. Future changes and health impacts of organic compounds

In the previous chapters I investigated the atmospheric impacts of organic compounds including VOCs and SOA on oxidant levels and associated chemical processes that affect air pollutants such as O_3, NO_2, SO_2, and fine PM. Multiple studies show that chronic exposure to these major air pollutants can cause severe cardiorespiratory (CR) diseases and is estimated to be responsible for premature deaths globally (Burnett *et al.*, 2014, 2018; Cohen *et al.*, 2017; Anenberg *et al.*, 2019). In this chapter, I utilized the model updates for gas and particle phase organic chemistry to investigate the present and future health impacts of organic compounds as an important driver in atmospheric chemistry.

The concentration-response factor (CRF) represents the relationship between pollutant exposure and health outcomes, and using an appropriate CRF is essential in estimating the health burden attributable to exposure to air pollutants. Systematic reviews on long-term exposure to pollutants including O_3, NO_2, and PM identified clear evidence of positive associations with cardiorespiratory mortality but also reported large heterogeneities of the CRFs of O_3 and NO_2 identified from various studies across the United States, Europe, Canada, China, and Japan (Chen and Hoek, 2020; Huangfu and Atkinson, 2020).

Despite the high levels of heterogeneity, previous studies have

commonly applied CRFs that were mainly based on North American or European cohorts to estimate the health outcomes in other global regions (Silva *et al.*, 2017; Park, Allen and Lim, 2020), including Korea (H. Kim, Kim and Lee, 2019; S. Kim, Kim and Lee, 2019). Bae and Kwon (2019) reviewed 27 published epidemiologic studies in Korea for the past two decades (1999 to 2018), which reported significant associations between long-term exposure to air pollution and mortality quantified by the relative risks (RR), hazard ratios (HR), and odds ratios (OR), but emphasized the necessity of additional cohort-based studies that can provide a more robust concentration-response relationship. As a follow-up, recent studies (Byun *et al.*, 2021, 2022; Kim *et al.*, 2021) based on Korean cohorts and health surveys have estimated age, cause, and region-specific RRs for use in the estimation of the health burden attributable to long-term exposure to O_3, NO_2, SO_2, and PM in Korea.

Future climate change, associated with changes in both meteorological variables and emissions, is expected to alter surface air quality. Most studies found that pollutant level changes in the future are mainly driven by the changes in precursor emissions (Kim *et al.*, 2015; Shim *et al.*, 2020; Thornhill *et al.*, 2021). Not only the changes in single pollutant concentrations but also the changes in the chemical composition of trace gases and particles in the atmosphere can affect future health outcomes. However, several Earth System Models (ESM) used in previous studies and future experiments therein often

implemented simplified chemistry schemes for efficiency (Kim *et al.*, 2015; Thornhill *et al.*, 2021; Lee *et al.*, 2022). Therefore, despite its computational cost, a more complex air quality model that can reflect both the anthropogenic and natural formation and degradation processes of secondary pollutants is necessary for more accurate estimations of future pollutant levels and understanding the chemical regimes and mechanisms that drive the changes.

In this chapter, I simulated air quality in Korea for the present and future conditions under different emission scenarios using GEOS-Chem. In particular, I used the most suitable approach to simulate gas and particle phase organic chemistry in Korea which were discussed in Chapters 2 and 3, incorporating a detailed aromatic chemistry mechanism and the aging Hodzic SOA scheme. Simulated results were used to estimate municipal-level O_3, NO_2, SO_2, and $PM_{2.5}$ attributable cardiorespiratory mortality changes using the CRFs based on recent Korean cohorts and health surveys, which can provide insight into the health benefits of future regulation policies.

4.1. Method

4.1.1. Model configuration

I used GEOS-Chem version 13.3.4 to simulate surface concentrations of O_3, NO_x, VOCs, SO_2, and $PM_{2.5}$ in Korea. Meteorological input (GEOS-FP assimilated meteorology), horizontal/vertical resolutions, and simulation domains of the global and nested simulations are identical as the description in Section 2.1.2. The model simulates more than 300 photochemical species, incorporating detailed aromatic VOC chemistry (Bates *et al*., 2021; Oak *et al*., 2019).

For SOA simulations, I used the aging Hodzic VBS scheme, which uses the VBS method with six bins and updated yield parameters that simulate high-NO_x and low-NO_x pathways of SOA formation (Hodzic *et al.*, 2016), and additional SOA aging to simulate functionalization (Jo *et al.*, 2013), which was found to be the most suitable approach in reproducing the formation and photochemical processing of observed SOA in Korea (Oak *et al.*, 2022). This SOA scheme simulates SOA formation from aromatic VOCs (AVOCs), S/IVOCs, and terpenes. For isoprene-derived SOA, I used an explicit mechanism based on Marais *et al*. (2016) instead of the VBS based method by Hodzic *et al*. (2016) and Pye *et al*. (2010). This method explicitly simulates the formation of low-volatility organics, including isoprene epoxydiol (IEPOX), which undergo irreversible aqueous-phase processes that occur more efficiently on acidic aerosol surfaces (Marais *et al.*, 2016).

Therefore, I define biogenic SOA (BSOA) as the sum of SOA derived by terpenes, simulated using the VBS approach, and by isoprene, simulated using the explicit aqueous-phase mechanism.

First I conducted the baseline simulation for 2019, representing present-day conditions. I used 2019 emissions from the Community Emissions Data System (CEDS) version 2 inventory for anthropogenic emissions (McDuffie *et al.*, 2020), MEGAN version 2.1 for biogenic emissions (Guenther *et al.*, 2012), and the Quick Fire Emissions Dataset (QFED) version 2.5 for biomass burning emissions (Darmenov and da Silva, 2015).

I conducted four additional simulations to compare the near-term and long-term changes under two Shared Socioeconomic Pathway (SSP) scenarios: SSP1, the most sustainable pathway with strong emissions control, and SSP3, the least sustainable scenario with mild regulations on anthropogenic emissions. I set the target years for the near-term and long-term future conditions to 2045 and 2095, respectively (Table 4.1). I fixed the meteorological fields to those of 2019 to eliminate the direct effect of meteorological change on pollutants such as wet and dry deposition, wind speed, temperature, humidity, etc., and focus on the changes in emissions and chemical formation. Future changes in land surface types and land use are also fixed to those of 2019. However, I took into account the future changes in biogenic emissions, which change from the vegetation response to temperature stress and CO_2 inhibition (Cao *et al.*, 2021), and changes in

methane (CH_4) concentrations due to climate change by applying scale factors to the present-day biogenic emissions and CH_4 levels based on previous studies (Saunois *et al.*, 2020; Turnock *et al.*, 2020; Cao *et al.*, 2021). For future anthropogenic and biomass burning emissions, I used projected emissions in the Coupled Model Intercomparison Project Phase 6 (CMIP6) and biomass burning emissions for CMIP6 (BB4CMIP) experiments (van Marle *et al.*, 2017; Gidden *et al.*, 2019). Emission totals of anthropogenic and biomass burning CO, NO_x, SO_2, POA, NMVOCs, and BVOCs (isoprene, monoterpenes, acetone, acetaldehyde, ethene, propene, ethanol, methanol) emissions in Northeast Asia (20−50°N, 100−140°E), and global CH_4 concentrations are summarized in Table 4.1.

Table 4.1. Annual emission totals in Northeast Asia and global CH_4 concentrations.

Category	Species	Present (2019)	SSP1 (2045)	SSP1 (2095)	SSP3 (2045)	SSP3 (2095)
Anthropogenic emissions [Tg]	CO	156	71	25	145	72
	NO_x	14.1	6.9	1.9	17.2	9.7
	SO_2	14.0	3.0	0.3	15.6	11.2
	POA	2.64	1.06	0.82	2.87	1.78
	NMVOCs	23.4	10.0	6.1	23.1	21.8
Biomass burning emissions [Tg]	CO	0.19	0.21	0.18	0.32	0.48
	POA	0.048	0.061	0.056	0.088	0.122
	NMVOCs	0.0014	0.0016	0.0014	0.0021	0.0028
Biogenic emissions [Tg]		21.8	24.4	23.6	24.6	29.1
Global CH_4 [ppbv]		1850	1580	2400	1080	3300

4.1.2. Premature mortality estimation

I used provincial-level (Korean; Si-Do) age-specific and cause-specific baseline mortality rates and municipal-level (Korean; Si-Gun-Gu) adult population in Korea for 2019 obtained from the Korean Statistical Information Service (KOSIS) portal (https://kosis.kr/eng/). I selected two cardiovascular disease categories: ischemic heart disease (IHD; KCD I20-I25) and other heart diseases (KCD I26-I51), and three respiratory disease categories: acute lower respiratory infection (ALRI; KCD J20-J22, U04), chronic obstructive pulmonary disease (COPD; KCD J40-J47), and other respiratory diseases (KCD J00-J98) for the calculation of premature deaths caused by air pollution.

According to Anenberg *et al*. (2010), long-term exposure to a pollutant is assumed to have a log-linear relationship with the relative risk, i.e., RR. The relative risk per Δx increase of pollutant concentration is an exponential function, as shown in Eq. (4.1), where β is the CRF, defined by the slope of the log-linear relation between the RR and pollutant concentration. The health outcome (Mort) is estimated using Eq. (4.2), where $Mort_{base}$ indicates the baseline mortality rate, Pop indicates the exposed adult (≥25 years) population, and AF is the attributable fraction of the pollutant. If the pollutant concentration (C) is below the threshold (C_{thres}), the AF is set to 0, but if $C \geq C_{thres}$, then the AF is defined as Eq. (4.3). The threshold values of each pollutant are summarized in Table 4.2.

Eq. (4.1) $RR = e^{\beta \Delta x}$

Eq. (4.2) $Mort = Mort_{base} \times Pop \times AF$

Eq. (4.3) $AF = \frac{RR-1}{RR} = 1 - \exp(-\beta \Delta C)$, where $\Delta C = C - C_{thres}$

To obtain the CRFs, i.e., β, I used Eq. (4.1) and RRs from recent epidemiologic studies in Korea, which estimated the association between long-term exposure to O_3, NO_2, SO_2, PM_{10}, and cardiorespiratory mortality using the Korean National Health and Nutritional Examination Survey (KNHANES) (Kim *et al.*, 2021) and the National Health Insurance Service-National Sample Cohort database (Byun *et al.*, 2021, 2022) along with air quality observations. Table 4.2 summarizes the cause and region-specific RRs and corresponding Δx of each pollutant used in this study.

The RRs of peak O_3 levels in a global meta-analysis review by Huangfu and Atkinson (2020) were 1.10 (95% CI: 1.03−1.18) and 1.02 (0.99−1.05) for ALRI and respiratory mortality, respectively. The results from Byun *et al*. (2022), which were used in this study, show larger RRs of 8-hour O_3 in Korea (Table 4.2). The RRs of NO_2 in the global meta-analysis were 1.03 (1.01−1.04), 1.06 (1.02−1.10), and 1.03 (1.00−1.05) for COPD, ALRI, and respiratory diseases. However, Table 4.2 shows that long-term exposure to NO_2 has a negative relationship with respiratory mortality in Korea. According to an ecological analysis of long-term exposure to air pollutants and cardiopulmonary mortality in Korea (Hwang *et al.*, 2020), NO_2 showed negative associations with pneumonia, 0.893 (0.861−0.923), and chronic

lower respiratory disease, 0.822 (0.780−0.865). Hwang *et al*. (2020) reported significant associations between cardiovascular diseases and long-term exposure to SO_2, with 1.09 (1.05−1.12) for IHD, but negative associations between respiratory diseases and SO_2, with 0.968 (0.943−0.994) for pneumonia, in Korea, which is consistent with the results from Kim *et al*. (2021), which were used in this study.

For calculating $PM_{2.5}$-attributable premature mortality, I used RRs estimated for PM_{10} due to the limited amount of long-term $PM_{2.5}$ observations in Korea (Byun *et al*., 2021). The combined RRs of PM_{10} and $PM_{2.5}$ in a meta-analysis review of approximately 20 studies on various global regions (Chen and Hoek, 2020) were 1.04 (0.99−1.10) and 1.11 (1.09−1.14), respectively, for circulatory diseases. For respiratory diseases, the RRs of PM_{10} and $PM_{2.5}$ were 1.12 (1.06−1.19) and 1.10 (1.03−1.18), respectively. Byun *et al*. (2021) noted that the RRs obtained from the Korean data are consistent with studies conducted in different countries. However, by incorporating Korean cohorts and PM data, the RRs of $PM_{2.5}$ used in this study represent the local characteristics and differences in PM levels, domestic population, and confounders, including income, drinking, smoking status, physical activity, and obesity.

While Pye *et al*. (2021) found significant associations between SOA and cardiorespiratory mortality in the US, Nault *et al*. (2021) and Ridley *et al*. (2017) estimated the potential health impacts of anthropogenic SOA and OA

using CTM simulations by multiplying the mass fraction of the component to $PM_{2.5}$ to the estimated $PM_{2.5}$-attributable mortality. In a similar matter, I applied the fractional method to estimate the mortality attributable to each chemical component of $PM_{2.5}$ ($Mort_{comp}$), by multiplying the total $PM_{2.5}$-attributable mortality ($Mort_{PM2.5}$) by the fraction of each component to total $PM_{2.5}$ ($C_{comp}/C_{PM2.5}$) as in Eq. (4.4).

Eq. (4.4) $Mort_{comp} = Mort_{PM2.5} \times C_{comp}/C_{PM2.5}$

For the estimation of future premature mortality under the SSPs, I used the 2019 baseline mortality rates. Assuming that the spatial distribution of the municipal-level population in the future is identical to that of 2019, I applied age-specific scale factors provided by the International Institute for Applied Systems Analysis (IIASA) SSP database (https://tntcat.iiasa.ac.at/SspDb) to the 2019 population data for each future scenario and year (KC and Lutz, 2017). Therefore, although future changes in the baseline mortality rates are neglected, I considered the changes in the total population and age structure. Figure 4.1 compares the adult population of 25 years and older and the age structure in the present and future scenarios. Population aging will be a common phenomenon under both scenarios, and the adult population will fall dramatically by 2095 under SSP3.

Table 4.2. RRs with 95% confidence intervals (CI) for cardiovascular and respiratory mortality per Δx increase of pollutants in Korea.

Pollutant	Threshold	Δx	Cardiovascular	Respiratory	Region	Reference
Annual mean	33.3 ppbv	10 ppbv	1.27	1.43	Nationwide	Byun *et al*.
MDA8 [a] O_3	(Anenberg *et al*., 2010)		(1.04−1.55)	(1.04−1.96)		(2022)
Annual mean	5.3 ppbv	11.41 ppbv	1.312	0.903	Nationwide	Kim *et al*.
NO_2	(WHO guideline)		(0.949−1.814)	(0.625−1.303)		(2021)
Annual mean	2 ppbv	2.09 ppbv	1.200	0.817	Nationwide	Kim *et al*.
SO_2	(Kim *et al*., 2021)		(0.960−1.500)	(0.589−1.133)		(2021)
Annual mean	5 μg m^{-3}	10 μg m^{-3}	1.244	1.166	Seoul metropolitan [b]	Byun *et al*.
$PM_{2.5}$	(WHO guideline)		(1.041−1.487)	(0.943−1.440)		(2021)
			1.211	1.466	Central [c]	
			(0.952−1.540)	(1.125−1.912)		

	0.840	0.905	Southern [d]
	(0.511−1.382)	(0.524−1.561)	
	1.053	1.171	Southeastern [e]
	(0.927−1.195)	(0.993−1.382)	
	1.136	1.118	Northeastern [f]
	(0.739−1.746)	(0.705−1.774)	

[a] Daily maximum 8-hour average

[b] Seoul, Incheon, Gyeonggi province

[c] Daejeon, Sejong, North Chungcheong province, South Chungcheong province, North Jeolla province

[d] Gwangju, South Jeolla province, Jeju

[e] Busan, Ulsan, Daegu, North Gyeongsang province, South Gyeongsang province

[f] Gangwon province

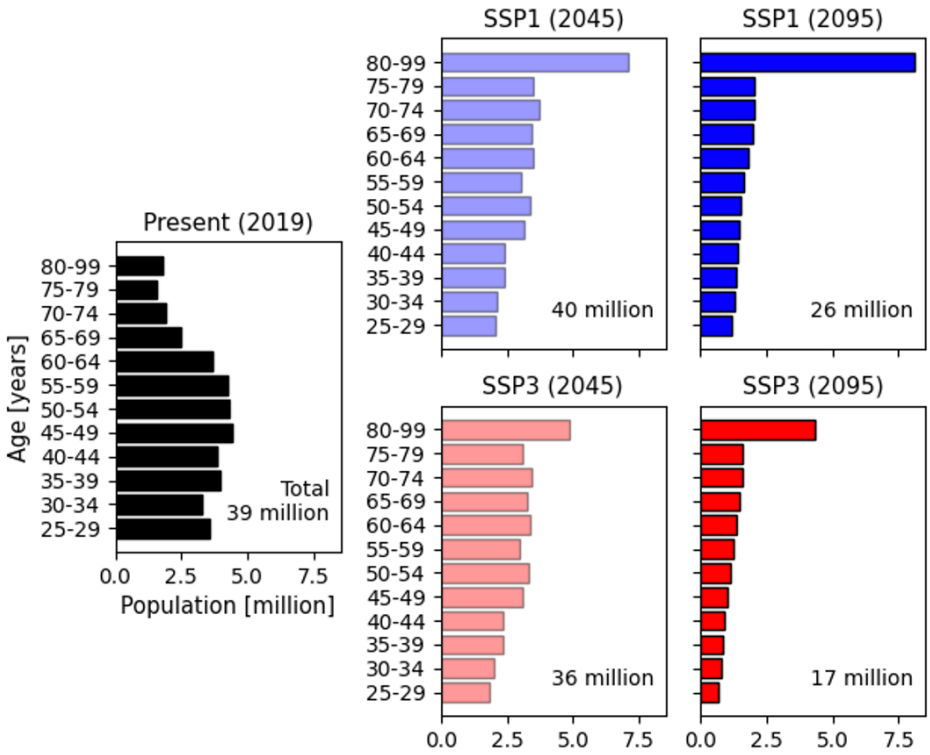

Figure 4.1. Age structure of total adult (25 ≥ years) population in Korea in 2019, and projected age structures for 2045 and 2095 under SSP1 and SSP3. Total adult population sizes are denoted in the lower-right corners.

4.2. Evaluation of present-day conditions

4.2.1. Present-day surface air quality

In this section, I evaluated GEOS-Chem's performance in simulating present-day conditions using hourly surface observations of O_3, NO_2, SO_2, and $PM_{2.5}$ at 419 AirKorea surface monitoring stations (https://www.airkorea.or.kr/eng/) during 2019. As the AirKorea network does not provide speciated $PM_{2.5}$ observations, I compared observed and simulated $PM_{2.5}$ chemical compositions at six supersites (Seoul, Daejeon, Gwangju, Ulsan, Baengnyeong, Jeju), which were provided by NIER. However, as continuous chemical composition observations at the six ground sites for 2019 were unavailable, I compared the seven-year averaged observations conducted from 2012 to 2018 with 2019 simulations.

Figure 4.2 compares observed and simulated MDA8 (daily maximum 8-hour average) O_3, daytime (06:00−18:00 LT) NO_2, SO_2, and $PM_{2.5}$ at AirKorea stations during 2019. I compared the daytime levels of NO_2, SO_2, and $PM_{2.5}$ to minimize the model-observation bias caused by the shallow nighttime PBL height in the model. While Oak *et al*. (2019) showed that GEOS-Chem underestimates the nighttime PBL by more than a factor of two compared to lidar-derived observations in Korea, this causes a rapid increase in simulated surface pollutant levels after sunset and a sharp decrease after sunrise. Therefore, I selected the 06:00−18:00 LT data for the analysis of NO_2, SO_2, and $PM_{2.5}$ below.

Figure 4.2a compares the monthly mean surface timeseries averaged over all AirKorea stations during 2019. The comparison shows that the model-observation biases for O_3, SO_2, and $PM_{2.5}$ are less than 10%, but a relatively large bias of −30% is shown in simulated NO_2 levels. This discrepancy may be attributable to interferences by non-NO_x reactive nitrogen species (NO_z) in the chemiluminescence monitors with molybdenum oxide converters that were used for measuring NO_2 (Dunlea *et al.*, 2007; Reed *et al.*, 2016). Although this interference is difficult to quantify using the available observations in this study, I find that simulated NO_z species, including PANs (peroxy acyl nitrates), nAPNs (non-acyl peroxy nitrates), N_2O_5, HNO_3, HONO, NO_3, and ANs (alkyl nitrates), especially NO_3, show non-negligible surface concentrations during the daytime in Korea. Comparison of the simulated sum of NO_2 and non-NO_x NO_z to measured NO_2 shows a model-observation bias of +16%. Therefore, I speculate that the magnitude of the bias for simulated NO_2 should lie within the range of −30% to +16%. While the model reproduces observed monthly variations of O_3, NO_2, and $PM_{2.5}$, with $R \geq 0.7$, the monthly variation of anthropogenic SO_2 emissions strongly resembles the simulated SO_2 timeseries, resulting in a relatively weak ($R = 0.59$) temporal correlation between observed and simulated monthly mean SO_2 compared to other species. The model generally captures the total amount and monthly variation of observed $PM_{2.5}$, with nitrate aerosols making up the largest portion among the simulated $PM_{2.5}$

components.

Figure 4.2b compares the spatial distributions of observed and simulated annual mean surface concentrations of air pollutants. AirKorea observations were regridded and interpolated to match the 0.25° latitude by 0.3125° longitude horizontal resolution for comparison with the model. The simulated spatial distribution of O_3 shows a weak correlation with observations compared to other species. The model overestimates O_3 in the Seoul metropolitan area, which is partly responsible for the regression slope of 0.4. A sensitivity test using different horizontal resolutions in the model showed that simulated surface daytime O_3 decreases by ~2% when using a finer model (9 km versus 3 km horizontal resolution) in Seoul (Hyeonmin Kim, personal communication, November 13, 2022), implying that the spatial resolution of the model can affect O_3 chemistry. The spatial correlation between observed and simulated SO_2 concentrations is lower (R = 0.46) compared to previous model simulations in Korea (R = 0.74) (Park *et al.*, 2021). A comparison of the KORUSv5 2016 emissions inventory used in Park *et al*. (2021) and CEDSv2 2019, which was used in this study, implies that the inaccurate representation of power plants and petrochemical complexes located along the western and southern coasts of the Korean peninsula, which serve as large point sources of SO_2 emissions in Korea (Chong *et al.*, 2020), is the main contributor to the discrepancy. The spatial distributions of observed NO_2 and $PM_{2.5}$ are well captured by the model, showing high values in urban and

industrial regions.

Figure 4.3 compares observed (2012-2018 mean) and simulated (2019) monthly mean surface timeseries of the major $PM_{2.5}$ chemical components: secondary inorganic aerosols ($SIA \equiv SO_4^{2-} + NO_3^- + NH_4^+$), BC or elemental carbon (EC), and OA at six ground sites. As the model simulates POC, I multiplied an organic aerosol to organic carbon ratio (OA/OC) of 1.3 for the conversion of POC to POA based on observations in East Asia (Philip *et al.*, 2014; Kim *et al.*, 2017; Kim, Zhang and Heo, 2018), and define modeled OA as the sum of POA and SOA (Oak *et al.*, 2022). I applied an OA/OC of 1.67 for January and October (Kim *et al.*, 2017), and 1.82 for April and July (Kim, Zhang and Heo, 2018) to the observed OC concentrations for comparison with the model.

Simulated SIA is overestimated compared to the seven-year average observations, especially during spring, due to the model's large nitrate (NO_3^-) composition (Figure 4.2a). Nitrate overestimation in East Asia has been commonly reported by air quality modeling studies (Choi *et al.*, 2019; Park *et al.*, 2021; Travis *et al.*, 2022; Zhai *et al.*, 2023). These studies suggest several missing sinks of nitrate and nitric acid in the model, including photolysis, dry and wet deposition, and uptake on anthropogenic coarse PM. The model-observation bias for monthly mean BC is 10%, and the model successfully simulates the monthly variation of observed BC. Simulated OA averaged at the six sites overestimates observations by 20%, and the model

fails to capture the seasonal variation of observed OA (R = −0.63). This is mainly due to the high bias of SOA during summer, likely caused by overestimated SOA aging, which was discussed in Section 3.3, and BSOA formation in the model. The conversion of measured OC to OA using constant OA/OC values may also serve as uncertainty that causes the bias.

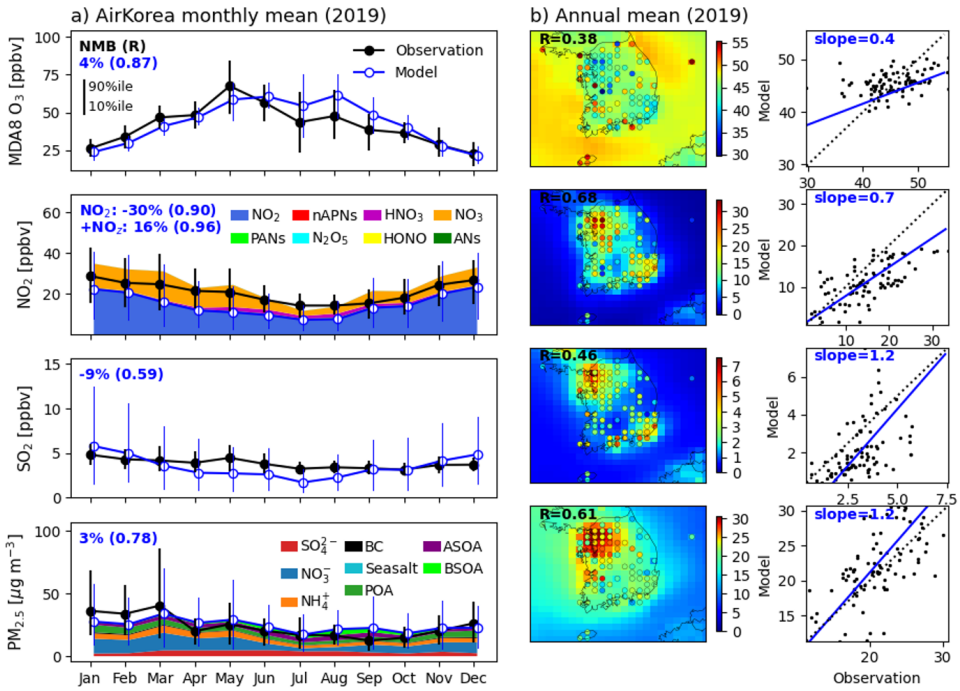

Figure 4.2. Observed and simulated a) monthly mean timeseries, b) annual mean spatial distribution and scatterplot comparison of MDA8 O_3, NO_2, SO_2, and $PM_{2.5}$ at AirKorea stations during 2019. Statistics (NMB, R) of model performance are denoted in the upper-left corners. Error bars indicate the 10th and 90th percentile values. Simulated NO_z species and chemical components of $PM_{2.5}$ in column a) are shown in different shades. Overlayed circles in column b) indicate the AirKorea observations regridded and interpolated to the model grid resolution.

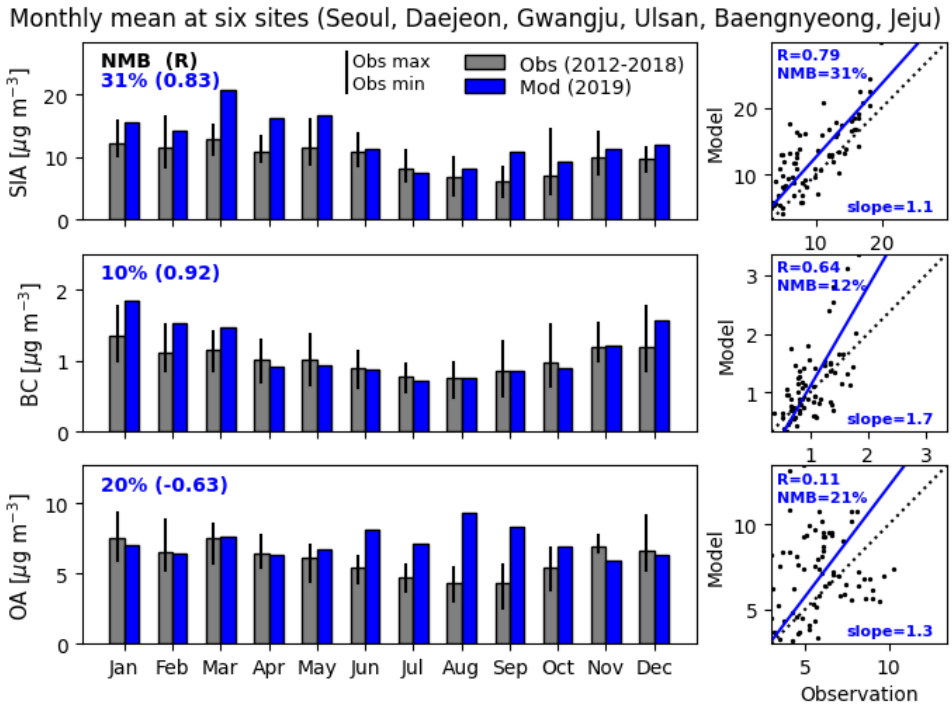

Figure 4.3. Observed (2012-2018 mean) and simulated (2019) monthly mean timeseries of major $PM_{2.5}$ chemical components at six supersites (Seoul, Daejeon, Gwangju, Ulsan, Baengnyeong, Jeju). The timeseries compare observed and simulated monthly mean values averaged at the six sites and error bars indicate the observed minimum and maximum values. The scatterplots compare observed and simulated monthly mean values at all of the six sites.

4.2.2. Present-day air pollution associated premature mortality

Here I will present estimated premature mortality attributable to each pollutant using individual RRs, but it should be noted that it is difficult to separate the independent health impact of each pollutant. As people are exposed to a mixture of pollutants in the real atmosphere, the combined effect of unknown chemicals that are co-emitted may be included in the results (Kim *et al.*, 2021).

The cardiovascular and respiratory mortality estimations with 95% confidence interval RRs due to long-term exposure to O_3, NO_2, SO_2, and $PM_{2.5}$ in Korea based on the AirKorea observations, are estimated to be 10419 (1271−17142), 8630 (0−18713), 3958 (0−9272), and 10431 (1411−20643) deaths in 2019 (Figure 4.4a). The spatial distribution of O_3-attributable deaths is relatively homogeneous compared to those of NO_2, SO_2, and $PM_{2.5}$, where the majority of deaths are located in the urban and industrial regions. Previous studies in Korea estimated 17224 (11056–22772) and 11924 (11649–12198) nationwide deaths attributable to $PM_{2.5}$ in 2013 (Kim *et al.*, 2018) and 2015 (Han *et al.*, 2018), when using RRs from North American cohorts and integrated exposure-response (IER) functions from Burnett *et al*. (2014). These estimates are higher than my results, as they included lung cancer mortality, which accounted for approximately 20% of total $PM_{2.5}$-attributable deaths.

The four air pollutants result in 26034 (1808−48316) cardiovascular and

7404 (874−17454) respiratory mortalities (Figure 4.4b), and a total of 33438 (2682−65770) deaths. I find similar estimates using simulated surface concentrations, sampled coherently in time and space with the observations, with 31151 (2887−60265) deaths.

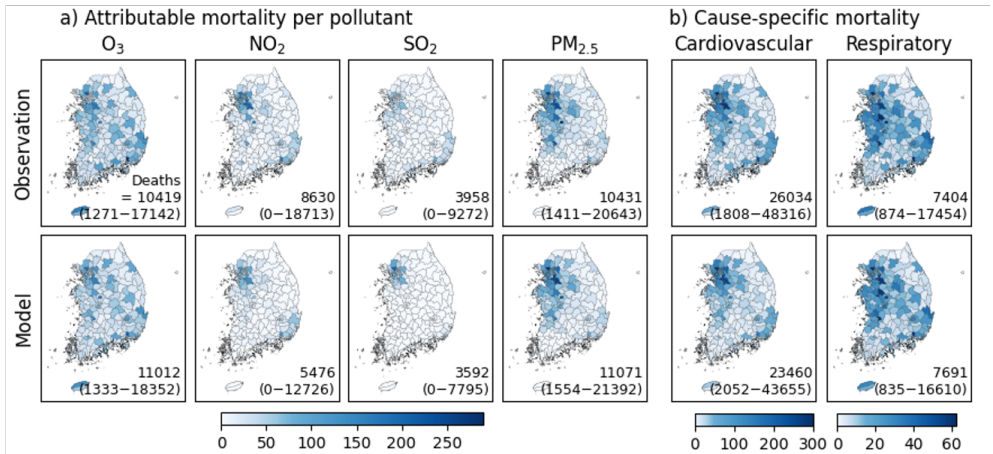

Figure 4.4. Spatial distributions of a) O_3, NO_2, SO_2, and $PM_{2.5}$ attributable mortality and b) total attributable cardiovascular and respiratory mortality estimated using observed and simulated surface concentrations, sampled coherently in time and space in Korea during 2019. Total deaths with estimations using 95% confidence interval RRs in parentheses are denoted in the lower-right corners.

4.2.3. Effect of aromatic chemistry to premature mortality

In this section, I estimated the effect of the detailed aromatic chemistry mechanism discussed in Chapter 2 to the pollution-attributable premature mortality in Korea during KORUS-AQ 2016. For mortality estimation I applied the method described in Section 4.1.2, but replaced the baseline mortality rates and adult population data to those of 2016.

Figure 4.5 shows the spatial distributions of MDA8 O_3, daytime NO_2, SO_2, and $PM_{2.5}$ concentrations and attributable premature mortality changes due to updated aromatic chemistry. As discussed in Chapter 2, surface O_3 levels increase and NO_2 levels decrease, as a result of increased NO_x recycling via aromatic oxidation. As OH levels increase along with the O_3 increase, the chemical loss of SO_2 increases, resulting in a slight decrease of SO_2. $PM_{2.5}$ levels increase throughout the country, which is due to increases in SIA. Increased oxidation of the SIA precursors, including SO_2 and NO_x, eventually increase aerosol formation. However, the aromatic chemistry mechanism implemented in Chapter 2 showed decreased AVOC levels (Figure 2.2), which results in a 5% decrease of SOA derived by AVOCs (ASOA).

The changes in premature mortality generally show linear responses to the changes in pollutant concentrations. My analysis shows that a total of 6589 annual deaths are responsible for aromatic chemistry in Korea. However, as I applied the KORUS-AQ campaign (May-June) averaged pollution levels, it should be noted that the annual deaths are likely overestimated, especially

for O_3. Nonetheless, the comparison implies that the health impact of aromatic chemistry cannot be neglected, and that changes in VOCs and NO_x emissions will play a critical role in modulating the chemical composition of the atmosphere. Therefore, in the following sections, I will investigate the health impact of future emissions changes of precursor species.

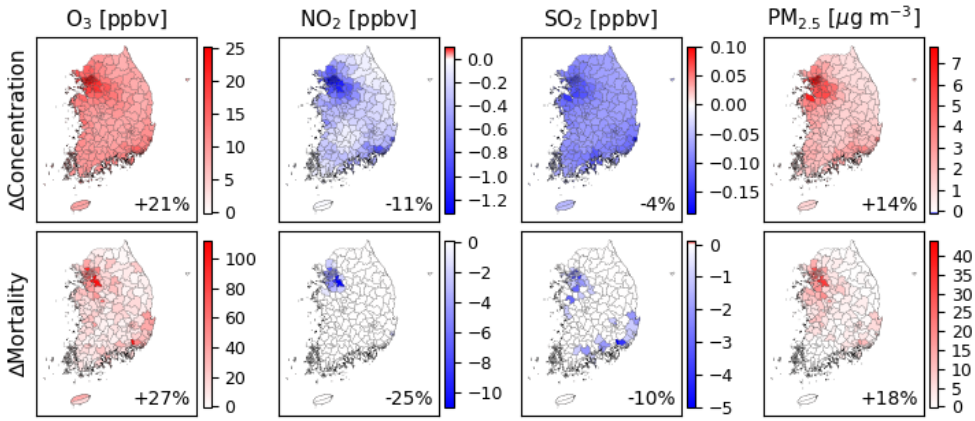

Figure 4.5. Spatial distributions of O_3, NO_2, SO_2, and $PM_{2.5}$ concentration and attributable premature mortality changes due to updated aromatic chemistry during KORUS-AQ 2016 (refer to Chapter 2). Relative changes ((AROM−BASE)/BASE) are denoted in the lower-right corners.

4.3. Future changes in air quality and premature mortality

4.3.1. Future changes in surface air quality

Gas species

Table 4.3 compares simulated annual mean pollutant concentrations in 2019 and the near-term and long-term future under the SSP1 and SSP3 scenarios. The near-term changes in O_3, NO_2, and SO_2 concentrations in Korea under the SSP1 scenario are −9%, −42%, and −52%, respectively. Under SSP3, pollutant concentrations change by +1%, +4%, and +22% in 2045. Long-term changes under the SSP1 scenario are −25%, −85%, and −85%, respectively, and under SSP3, concentrations change by +9%, −36%, and +7% in 2095, respectively.

O_3 change is mainly associated with decreases in precursor concentrations due to strong regulations on anthropogenic emissions under SSP1. However, O_3 is sensitive to increased biogenic emissions in warmer climates and higher CH_4 levels under SSP3. I find that O_3 formation in Korea occurs in a NO_x-limited regime (VOCs/NO_x > 10 ppbC/ppbv) in 2095 under SSP1, with significant increases in VOCs/NO_x ratios (Figure 4.6) in the regions where O_3 levels decrease. Under SSP3, VOCs/NO_x ratios indicate that most regions in the country will be VOC-limited (VOCs/NO_x ≈ 10 ppbC/ppbv) in 2095. NO_2 levels decrease in 2095 regardless of scenarios due to changes in primary emissions, but the magnitude of emissions reduction is a factor of three higher in SSP1, resulting in lower surface concentrations by a factor of

four than in SSP3. Similarly, SO_2 decreases in 2095 by more than 50% compared to the present under SSP1. However, SO_2 increases as SO_2 emissions remain nearly unchanged, and oxidant (OH) levels decrease due to the chemical loss by CH_4 (Figure 4.6) under SSP3.

Kim *et al*. (2015) used a coupled chemistry-climate model and simulated an increase in surface O_3 in East Asia in 2050 relative to 2000 under the Representative Concentration Pathway (RCP) 8.5 scenario and O_3 decreases in all other RCP scenarios. The multi-model mean of six CMIP6 models estimated a decrease by ~15 ppbv and an increase by ~6 ppbv in annual O_3 concentrations in East Asia in 2100 relative to the 2005−2014 mean value (Turnock *et al.*, 2020), displaying similar tendencies with my future simulations.

Aerosol species

Simulated annual mean aerosol concentrations, including $PM_{2.5}$, SIA, and ASOA and SOA from BVOCs (BSOA), are summarized in Table 4.3. $PM_{2.5}$ concentrations change by −49% and +7% in 2045 under SSP1 and SSP3, respectively, but eventually decrease by 72% and 17% in both scenarios. Simulated results suggest that under the SSP1 scenario, Korea will meet close to the WHO annual mean $PM_{2.5}$ standard of 5 μg m^{-3} in 2095.

As most anthropogenic emissions decrease in future scenarios, primary aerosols (BC, POA) and SIA concentrations decrease in the long-term under both SSP1 and SSP3. Future SOA concentrations decrease compared to

present-day levels, but the contribution of BSOA to total $PM_{2.5}$ increases, especially along the middle parts of the country (not shown), where most biogenic sources are located. I find that the anthropogenic emissions decrease contributes to the decrease in the major $PM_{2.5}$ components, including SIA, ASOA, and BSOA.

OH, O_3 and NO_3 are the major oxidants that react with BVOCs (isoprene and monoterpenes), and their SOA yields are sensitive to NO_x levels (Pye *et al.*, 2010). Significant reductions in NO_x emissions in 2095 under SSP1 substantially decrease O_3 and NO_3 levels by up to −90% (Figure 4.6), resulting in higher BVOC concentrations compared to 2019. Similar results were reported by Jo *et al*. (2019), where they found an increase in isoprene under a 50% decrease in NO_x and SO_2 emissions. Despite the increase in BVOC levels under SSP1, the reduction of NO_x and SO_2 decreases sulfate aerosol levels, increases aerosol pH, and decreases BSOA formation. My results are consistent with the previous studies (Dong *et al*., 2022; Jo *et al*., 2019), which found suppressed aqueous phase formation of BSOA under reduced anthropogenic emissions. I also find that the change in BSOA is approximately proportional to the change in SIA concentrations under SSP1. Under SSP3, the effect of increased BVOC emissions and CH_4 levels on BSOA formation is more significant than anthropogenic emissions reduction, resulting in a net increase in BSOA in 2095.

Estimated future changes in $PM_{2.5}$ concentrations simulated by a fully-

coupled ESM (Sellar *et al.*, 2019) are consistent with the results presented in Table 4.3. Shim *et al*. (2020) show that the annual mean $PM_{2.5}$ concentration in East Asia will drop to 10 μg m^{-3} in 2035 and remain at approximately 6 μg m^{-3} between 2081 to 2100 under SSP1. Under SSP3, $PM_{2.5}$ will reach up to 25 μg m^{-3} around 2050 and slowly decrease to 18 μg m^{-3} in 2100. My results showing a decrease in SOA concentrations by 2.4 and 0.2 μg m^{-3} in 2095 relative to 2019 under SSP1 and SSP3, respectively, are also comparable to the results by Lin *et al*. (2016), where they estimated an SOA decrease of ~1 μg m^{-3} in Northeast Asia in 2100 relative to 2000 under the RCP8.5 scenario using the Community Earth System Model (CESM).

Table 4.3. Simulated annual mean O_3, NO_2, SO_2, $PM_{2.5}$, SIA, and SOA (aromatic and biogenic) concentrations in 2019 and the near-term and long-term future under the SSP1 and SSP3 scenarios. Relative changes ((future−present)/present) are denoted in parentheses.

Species	Present (2019)	SSP1 (2045)	SSP1 (2095)	SSP3 (2045)	SSP3 (2095)
O_3 [ppbv]	44.9	41.0 (−9%)	33.8 (−25%)	45.5 (+1%)	49.0 (+9%)
NO_2 [ppbv]	12.3	7.1 (−42%)	1.8 (−85%)	12.8 (+4%)	7.9 (−36%)
SO_2 [ppbv]	2.7	1.3 (−52%)	0.4 (−85%)	3.3 (+22%)	2.9 (+7%)
$PM_{2.5}$ [μg m^{-3}]	21.7	11.1 (−49%)	6.1 (−72%)	23.3 (+7%)	18.1 (−17%)
SIA [μg m^{-3}]	14.3	6.9 (−52%)	1.9 (−87%)	15.6 (+9%)	12.5 (−13%)
ASOA [μg m^{-3}]	2.7	1.6 (−41%)	0.7 (−74%)	2.4 (−11%)	2.1 (−22%)
BSOA [μg m^{-3}]	1.9	1.6 (−16%)	1.5 (−21%)	2.1 (+11%)	2.3 (+21%)

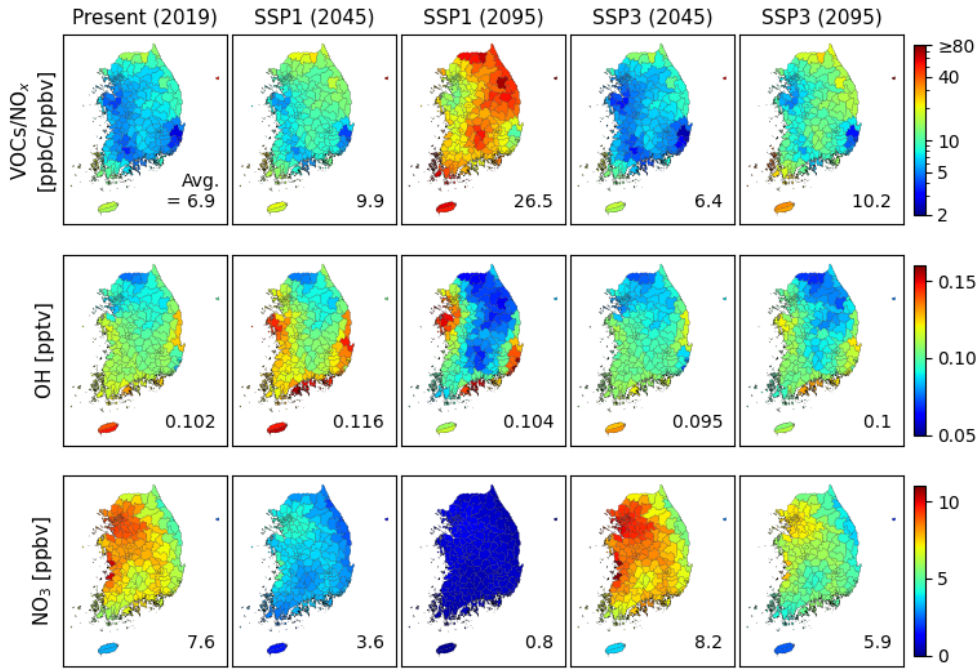

Figure 4.6. Simulated annual mean $VOCs/NO_x$ ratios, OH, and NO_3 concentrations in the present, near-term, long-term future under SSP1 and SSP3 in Korea. The average values (Avg.) are denoted in the lower-right corners.

4.3.2. Future changes in air pollution associated premature mortality

Kim *et al*. (2020) estimated a total of 25400 (23400−56600) O_3 and $PM_{2.5}$ attributable to premature mortality in Korea in 2005, comparable to my estimation of 20850 in 2019. They estimated a future decrease of 20000 annual deaths in 2050 under the SSP2 scenario, which assumes moderate socioeconomic growth and lies in between the SSP1 and SSP3 pathways, and 10100 deaths under the SSP3 scenario. In this section, I will discuss estimated future changes in premature mortality under the SSP1 and SSP3 scenarios using the future simulation results.

Figure 4.7a compares the nationwide total premature mortality due to O_3, NO_2, SO_2, and $PM_{2.5}$ (≡ SIA + ASOA + BSOA + BC + POA + etc.) exposure under present and future conditions in Korea. As the future population and age structure change differently under each scenario (Figure 4.1), this effect is reflected in the estimated mortality as expressed in Eq. (4.2). Figure 4.7b quantifies the different effects of pollutant concentration change and population change on future changes in premature mortality.

Estimated total cardiorespiratory excess mortality due to air pollutants shows a slight decrease (−8%) under SSP1 for the near-term future but eventually decreases by 95% in 2095. Figure 4.7b shows that the effects of pollutant level decrease and population structure change are comparable, but the pollutant effect outweighs the population effect, resulting in a net decrease in premature mortality in the near-term future under SSP1. In the long-term

future, a successful reduction in pollutant levels results in a decrease in premature mortality.

Under SSP3, estimated excess mortality increases by 80% in 2045, and decreases by 22% in 2095, compared to the present. As the future pollution levels will be similar to or slightly lower than that of the present, the aging population under SSP3 will be the leading cause of increased premature deaths in the near-term future. Figure 4.7b shows that Korea will benefit from improved air quality in the long-term under both the SSP1 and SSP3 scenarios, but the effect of pollutant level decrease greatly differs depending on the future scenario (−96% versus −2%).

The long-term health burden of individual chemical components comprising $PM_{2.5}$ may differ, but it is difficult to quantify due to the lack of long-term observations. Therefore, most epidemiologic studies estimated the association between total PM mass and premature mortality in Korea (Byun *et al.*, 2021). However, as the relative abundance of simulated BSOA among the major components increases by at least a factor of ~2.5 in 2095 under SSP1(Oak *et al.*, 2023), especially in the Northeastern region, this emphasizes the potential health burden of BSOA on a local scale in the future.

Figure 4.8 shows the estimated premature mortality attributable to each $PM_{2.5}$ component using the fractional method expressed as in Eq. (4.4). Under SSP1, while the total $PM_{2.5}$-attributable mortality in 2095 dramatically decreases, the contribution of BSOA to total $PM_{2.5}$ is more significant than

that of ASOA, and the overall health impact of SOA (ASOA + BSOA) is comparable to that of SIA. The changes in ASOA and POA attributable mortality follow the changes in anthropogenic emissions, showing the largest decrease under SSP1. Under SSP3, SIA comprises more than half of the total $PM_{2.5}$ mass in 2095, with a relatively homogeneous spatial distribution (Oak *et al.*, 2023). This results in the largest contribution of SIA to total $PM_{2.5}$-attributable mortality. Although ASOA and POA attributable mortality decrease in the long-term, BSOA-attributable mortality increases by ~50% in 2095 under SSP3. As a result, the changes in SOA concentrations cause a ~20% increase in attributable cardiorespiratory deaths.

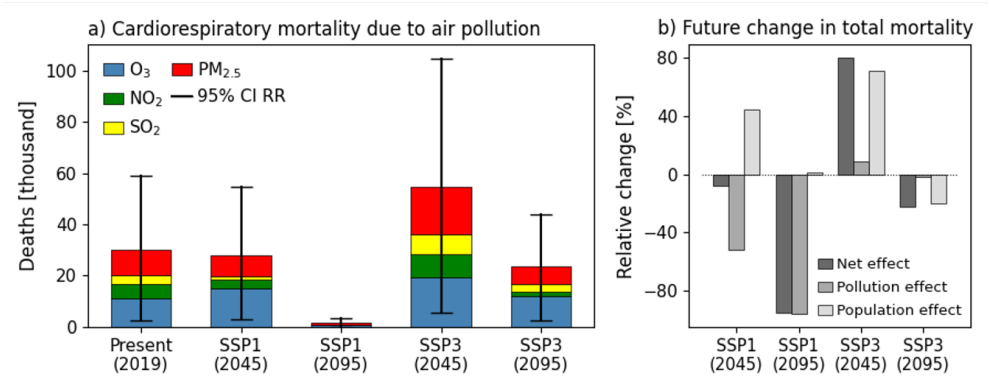

Figure 4.7. Estimated a) premature mortality due to O_3, NO_2, SO_2, and $PM_{2.5}$ long-term exposure, and b) present to future relative changes ((future−present)/present) in total premature mortality due to O_3, NO_2, SO_2, and $PM_{2.5}$ under the SSPs in Korea. In panel a), each bar in different shades indicates the mortality attributable to each pollutant, and the error bars indicate estimations of total mortality using 95% confidence interval RRs. In panel b), each bar in different shades indicates the future changes in response to pollutant concentration change, population and age structure change, and the net effect.

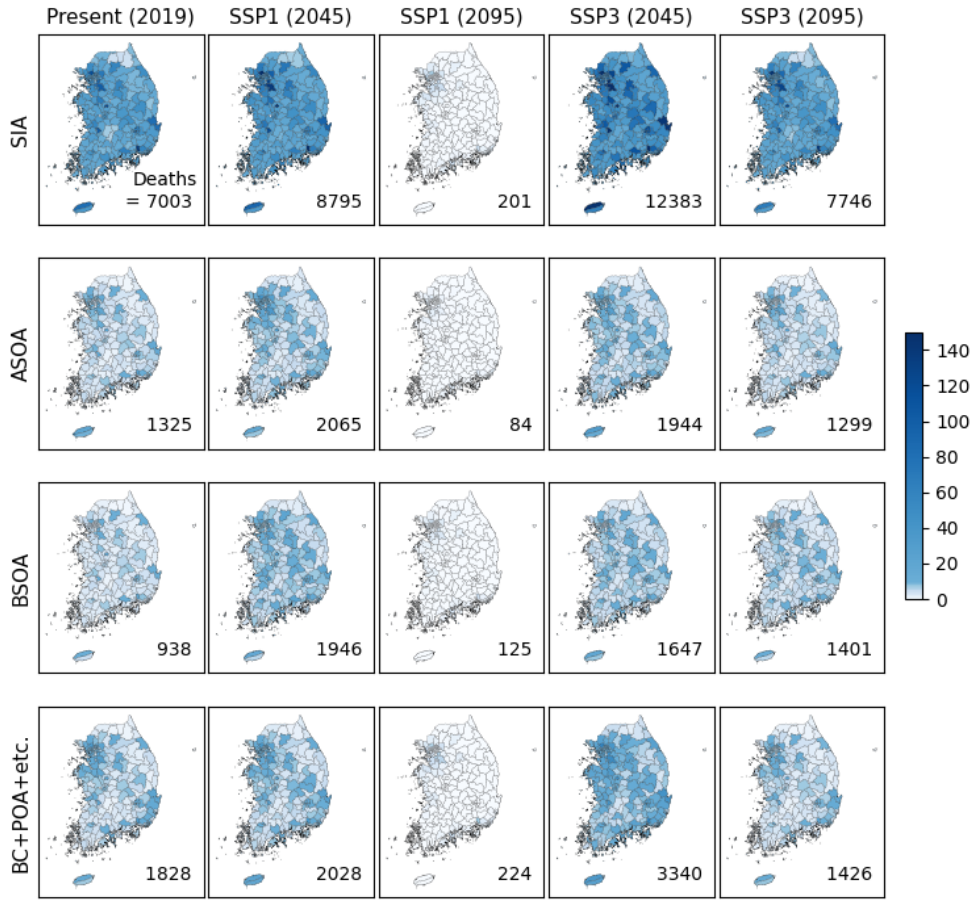

Figure 4.8. Estimated premature mortality due to the major components of $PM_{2.5}$ (SIA, ASOA, BSOA, and BC + POA + etc.) in the present, near-term, long-term future under SSP1 and SSP3 in Korea. Total deaths are denoted in the lower-right corners.

4.4. Summary and discussion

I analyzed future changes in O_3, NO_2, SO_2, and $PM_{2.5}$ concentrations and their cardiorespiratory health burden relative to the present in Korea by using CRFs based on Korean cohorts and health surveys, and GEOS-Chem with updated aromatic chemistry and SOA treatments. The health impact of aromatic chemistry was responsible for a ~21% increase in estimated premature mortality in Korea during KORUS-AQ 2016. I considered future changes in anthropogenic and natural emissions under SSP1 and SSP3 based on CMIP6 experiments, and the future population and age structures in Korea from the SSP database.

Significant reductions in precursor emissions under the SSP1 scenario will decrease future concentrations of most gas and aerosol species compared to the present. The improvement in air quality will eventually lead to a large decrease (−94%) in premature mortality in 2095. Despite the decrease in total mortality, the relative abundance of BSOA among the major components of $PM_{2.5}$ emphasizes the need to consider BSOA and its health impact on a local scale in the future.

Under the SSP3 scenario, O_3 will increase in the future, mainly driven by increased biogenic emissions under the warming climate. Concentrations of NO_2, SO_2, SIA, POA, and ASOA generally follow the trends in anthropogenic emissions change. In the long-term future, pollutant concentrations will be similar to or slightly lower than that of the present. The

aging population under SSP3 will cause increased premature deaths in the near future, but the decrease in the total adult population will decrease premature mortality by 22% in 2095. However, SOA-attributable cardiorespiratory deaths will increase by ~20%.

The application of the RRs estimated for PM_{10} to calculate premature mortality attributable to $PM_{2.5}$ and its chemical components serves as a major limitation of this study. $PM_{2.5}$ is more likely to reach deeper into the circulatory or respiratory system (Oberdörster, Oberdörster and Oberdörster, 2005) with larger toxicity than PM_{10} (Kelly and Fussell, 2012), which may imply a larger RR for $PM_{2.5}$ (Yorifuji *et al.*, 2015). The fractional method used for estimating the health burden of individual chemical components comprising $PM_{2.5}$ also holds uncertainties, because the size distribution and chemical nature differ among components. Continuous long-term observations should be conducted and analyzed to estimate component-specific or size-specific RRs in future epidemiologic studies in Korea.

Lastly, I estimated mortality attributable to each pollutant using species-specific RRs, but exposure to a mixture of pollutants that are co-emitted can simultaneously affect the human cardiorespiratory system (Kim *et al.*, 2021). Therefore, uncertainties should be noted when interpreting the estimated health impact of each pollutant. Nonetheless, this study implies a substantial difference in the long-term health outcomes in Korea depending on the future scenario and provide insight into the efficacy of future regulation policies.

Chapter 5. Summary and conclusions

Sources and fates of atmospheric organic compounds are essential in the formation of secondary air pollutants and modulating the oxidation capacity of the atmosphere, and can cause in severe damage to the human cardiorespiratory system. This dissertation aims to improve scientific understanding of the atmospheric role and potential impacts of gas/particle phase organic chemistry in Korea by utilizing a chemical transport model and investigating the effect of gas phase aromatic chemistry on tropospheric O_3 and oxidants, the chemical/physical formation and loss processes of organic aerosols, and finally the future changes and health impacts of organic compounds.

In Chapter 2, model evaluation between simulated OPE using a 3-D CTM (GEOS-Chem) and an observation-constrained 0-D box model showed that aromatic chemistry can increase the average net O_3 production in Korea by 37% during the springtime. The implementation of a detailed aromatic chemistry scheme in the model increased simulated O_3 levels by 13%, driven by increased NO_x recycling. Sensitivity tests with the updated aromatic chemistry scheme showed that without VOCs reduction, NO_x reduction alone can result in significant increases in O_3 levels in urban and industrial regions, implying the importance of concurrent emission reductions for both NO_x and VOCs in order to effectively reduce O_3 levels in Korea. Chapter 2 emphasized the role of gas phase aromatic chemistry in producing secondary pollutants in

Korea regarding the relative abundance and reactivities of aromatics. The estimated the health impact of aromatic chemistry in Chapter 4 showed that it was responsible for a ~21% increase in estimated premature mortality in Korea during KORUS-AQ 2016.

In Chapter 3, I examined the role of aromatics as a precursor of particle formation in urban environments in Korea. I compared four different SOA schemes (Complex, Simple, Hodzic, Jo) using GEOS-Chem during spring-summer 2016 and fall-winter 2017/2018 in Seoul. During the spring-summer seasons, the Jo scheme simulated the highest SOA concentrations, owing to chemical aging processes, followed by the Simple and Hodzic schemes. The Complex scheme underestimated observed SOA concentrations compared to the Hodzic and Jo schemes, regardless of seasons, indicating the necessity of additional SOA precursors. The Simple scheme simulated the largest amounts during fall-winter, followed by the Jo and Hodzic schemes. For better model representation of SOA formation in urban environments such as in Seoul, this study suggests the inclusion of additional S/IVOCs precursors and chemical aging processes of SOA. In terms of reproducing the photochemical characteristics of observed surface SOA in Seoul, the aging Hodzic scheme (Hodzic VBS + SOA aging) showed good performance. However, the SOA yields used in the Hodzic VBS framework may result in an overprediction of chemical aging. Therefore, different yield parameters (e.g., thermodenuder-derived yields) that are applicable to the explicit SOA aging scheme in the

model should be further tested.

In Chapter 4, I utilized the model updates for gas and particle phase organic chemistry to investigate the health impacts of organic compounds as an important driver in atmospheric chemistry. I analyzed near-term (2045) and long-term (2095) future changes of O_3, NO_2, SO_2, and $PM_{2.5}$ concentrations and their cardiorespiratory health burden in Korea by using CRFs based on Korean cohorts and health surveys, and GEOS-Chem with updated aromatic chemistry and SOA treatments (Hodzic VBS + SOA aging). I considered future changes in anthropogenic and natural emissions, population, and age structures under SSP1 and SSP3 scenarios. Significant reductions in precursor emissions under the SSP1 scenario substantially improves air quality, which will eventually lead to a large decrease (−94%) in premature mortality in 2095. Despite the decrease in premature mortality, the relative abundance of BSOA among the major components of $PM_{2.5}$ emphasizes the need to consider BSOA and its health impact on a local scale in the future under the warming climate. Under the SSP3 scenario, O_3 will increase, mainly driven by increased biogenic emissions in the future climate. In the long-term future, overall pollutant concentrations will be similar to or slightly lower than that of the present. While pollutant levels drive the premature mortality changes under SSP1, the aging population under SSP3 will cause increased premature deaths in the near future, but the decrease in the total adult population will decrease premature mortality in 2095. However,

the changes in SOA concentrations, especially the increase of BSOA, will cause a ~20% increase in SOA-attributable cardiorespiratory deaths under SSP3. This implies a substantial difference in the long-term health outcomes in Korea depending on the future emission and population scenario and can provide insight into the efficacy of future regulation policies. The results in this dissertation can be considered in establishing control strategies for the future, especially in terms of adaptation and mitigation of climate change.

Bibliography

Anenberg, S. C. *et al.* (2010) 'An estimate of the global burden of anthropogenic ozone and fine particulate matter on premature human mortality using atmospheric modeling', *Environmental Health Perspectives*, 118(9), pp. 1189–1195. doi: 10.1289/ehp.0901220.

Anenberg, S. C. *et al.* (2019) *Pollution-related health impacts of transportation sector emission in 2010 and 2015*, *ICCT, Clim. Clean Air Coal.*

Atkinson, R. (2000) 'Atmospheric chemistry of VOCs and NOx', *Atmospheric Environment*, 34(12), pp. 2063–2101. doi: https://doi.org/10.1016/S1352-2310(99)00460-4.

Bae, S. and Kwon, H. J. (2019) 'Current state of research on the risk of morbidity and mortality associated with air pollution in korea', *Yonsei Medical Journal*. Yonsei University College of Medicine, pp. 243–256. doi: 10.3349/ymj.2019.60.3.243.

Bates, K. H. *et al.* (2021) 'Development and evaluation of a new compact mechanism for aromatic oxidation in atmospheric models', *Atmos. Chem. Phys.*, 21(24), pp. 18351–18374. doi: 10.5194/acp-21-18351-2021.

Bey, I. *et al.* (2001) 'Global modeling of tropospheric chemistry with assimilated meteorology: Model description and evaluation', *Journal of Geophysical Research: Atmospheres*, 106(D19), pp. 23073–23095. doi: 10.1029/2001JD000807.

Burnett, R. *et al.* (2014) 'An Integrated Risk Function for Estimating the

Global Burden of Disease Attributable to Ambient Fine Particulate Matter Exposure', *Environmental health perspectives*, 122. doi: 10.1289/ehp.1307049.

Burnett, R. *et al.* (2018) 'Global estimates of mortality associated with longterm exposure to outdoor fine particulate matter', *Proceedings of the National Academy of Sciences of the United States of America*, 115(38), pp. 9592–9597. doi: 10.1073/pnas.1803222115.

Byun, G. *et al.* (2021) 'Health and Economic Burden Attributable to Particulate Matter in South Korea: Considering Spatial Variation in Relative Risk', *Journal of Environmental Health Sciences*. 2021/10/31, 47(5), pp. 486–495. doi: 10.5668/JEHS.2021.47.5.486.

Byun, G. *et al.* (2022) 'Long-term exposure to ambient ozone and mortality in a population-based cohort of South Korea: Considering for an alternative exposure time metric', *Environmental Pollution*, 314, p. 120300. doi: https://doi.org/10.1016/j.envpol.2022.120300.

Cao, Y. *et al.* (2021) 'Ensemble projection of global isoprene emissions by the end of 21st century using CMIP6 models', *Atmospheric Environment*, 267, p. 118766. doi: https://doi.org/10.1016/j.atmosenv.2021.118766.

Carmichael, G. R. *et al.* (2008) 'MICS-Asia II: The model intercomparison study for Asia Phase II methodology and overview of findings', *Atmospheric Environment*, 42(15), pp. 3468–3490. doi: https://doi.org/10.1016/j.atmosenv.2007.04.007.

Chacon-Madrid, H. J. and Donahue, N. M. (2011) 'Fragmentation vs. functionalization: chemical aging and organic aerosol formation', *Atmos. Chem. Phys.*, 11(20), pp. 10553–10563. doi: 10.5194/acp-11-10553-2011.

Chang, K.-L. *et al.* (2019) 'A new method (M3Fusion v1) for combining observations and multiple model output for an improved estimate of the global surface ozone distribution', *Geosci. Model Dev.*, 12(3), pp. 955–978. doi: 10.5194/gmd-12-955-2019.

Chen, J. and Hoek, G. (2020) 'Long-term exposure to PM and all-cause and cause-specific mortality: A systematic review and meta-analysis', *Environment International*, 143, p. 105974. doi: https://doi.org/10.1016/j.envint.2020.105974.

Choi, J. *et al.* (2019) 'Impacts of local vs. trans-boundary emissions from different sectors on PM2.5 exposure in South Korea during the KORUS-AQ campaign', *Atmospheric Environment*, 203, pp. 196–205. doi: 10.1016/j.atmosenv.2019.02.008.

Chong, H. *et al.* (2020) 'High-resolution mapping of SO2 using airborne observations from the GeoTASO instrument during the KORUS-AQ field study: PCA-based vertical column retrievals', *Remote Sensing of Environment*, 241, p. 111725. doi: 10.1016/j.rse.2020.111725.

Cohen, A. J. *et al.* (2017) 'Estimates and 25-year trends of the global burden of disease attributable to ambient air pollution: an analysis of data from the Global Burden of Diseases Study 2015', *The Lancet*, 389(10082),

pp. 1907–1918. doi: 10.1016/S0140-6736(17)30505-6.

Cooke, W. *et al.* (1999) 'Construction of a 1° × 1° fossil fuel emission data set for carbonaceous aerosol and implementation and radiative impact in the ECHAM4 model', *Journal of Geophysical Research: Atmospheres*, 104(D18), pp. 22137–22162. doi: 10.1029/1999jd900187.

Crawford, J. H. *et al.* (2021) 'The Korea-United States Air Quality (KORUS-AQ) Field Study', *Elem Sci Anth*.

Crouse, D. L. *et al.* (2015) 'Ambient PM2.5, O3, and NO2 exposures and associations with mortality over 16 years of follow-up in the canadian census health and environment cohort (CanCHEC)', *Environmental Health Perspectives*, 123(11), pp. 1180–1186. doi: 10.1289/ehp.1409276.

Darmenov, A. and da Silva, A. (2015) *The quick fire emissions dataset (QFED) – Documentation of versions 2.1, 2.2 and 2.4*.

DeCarlo, P. F. *et al.* (2006) 'Field-Deployable, High-Resolution, Time-of-Flight Aerosol Mass Spectrometer', *Analytical Chemistry*, 78(24), pp. 8281–8289. doi: 10.1021/ac061249n.

Donahue, N. M. *et al.* (2006) 'Coupled Partitioning, Dilution, and Chemical Aging of Semivolatile Organics', *Environmental Science & Technology*, 40(8), pp. 2635–2643. doi: 10.1021/es052297c.

Donahue, N. M. *et al.* (2013) 'How do organic vapors contribute to new-particle formation?', *Faraday Discussions*, 165(0), pp. 91–104. doi: 10.1039/C3FD00046J.

Dong, X. *et al.* (2022) 'Modeling Analysis of Biogenic Secondary Organic Aerosol Dependence on Anthropogenic Emissions in China', *Environmental Science & Technology Letters*, 9(4), pp. 286–292. doi: 10.1021/acs.estlett.2c00104.

Dunlea, E. J. *et al.* (2007) 'Evaluation of nitrogen dioxide chemiluminescence monitors in a polluted urban environment', *Atmos. Chem. Phys.*, 7(10), pp. 2691–2704. doi: 10.5194/acp-7-2691-2007.

Farina, S. C., Adams, P. J. and Pandis, S. N. (2010) 'Modeling global secondary organic aerosol formation and processing with the volatility basis set: Implications for anthropogenic secondary organic aerosol', *Journal of Geophysical Research: Atmospheres*, 115(D9). doi: https://doi.org/10.1029/2009JD013046.

Faustini, A., Rapp, R. and Forastiere, F. (2014) 'Nitrogen dioxide and mortality: Review and meta-analysis of long-term studies', *European Respiratory Journal*. European Respiratory Society, pp. 744–753. doi: 10.1183/09031936.00114713.

Gaubert, B. *et al.* (2020) 'Correcting model biases of CO in East Asia: impact on oxidant distributions during KORUS-AQ', *Atmos. Chem. Phys. Discuss.*, 2020, pp. 1–49. doi: 10.5194/acp-2020-599.

Gidden, M. J. *et al.* (2019) 'Global emissions pathways under different socioeconomic scenarios for use in CMIP6: a dataset of harmonized emissions trajectories through the end of the century', *Geosci. Model Dev.*,

12(4), pp. 1443–1475. doi: 10.5194/gmd-12-1443-2019.

Glasius, M. and Goldstein, A. H. (2016) 'Recent Discoveries and Future Challenges in Atmospheric Organic Chemistry', *Environmental Science & Technology*, 50(6), pp. 2754–2764. doi: 10.1021/acs.est.5b05105.

Goldberg, D. L. *et al.* (2019) 'A top-down assessment using OMI NO2 suggests an underestimate in the NOx emissions inventory in Seoul, South Korea, during KORUS-AQ', *Atmos. Chem. Phys.*, 19(3), pp. 1801–1818. doi: 10.5194/acp-19-1801-2019.

de Gouw, J. and Jimenez, J. L. (2009) 'Organic Aerosols in the Earth's Atmosphere', *Environmental Science & Technology*, 43(20), pp. 7614–7618. doi: 10.1021/es9006004.

Griffin, R. J. *et al.* (1999) 'Organic aerosol formation from the oxidation of biogenic hydrocarbons', *Journal of Geophysical Research: Atmospheres*, 104(D3), pp. 3555–3567. doi: https://doi.org/10.1029/1998JD100049.

Guenther, A. B. *et al.* (2012) 'The Model of Emissions of Gases and Aerosols from Nature version 2.1 (MEGAN2.1): an extended and updated framework for modeling biogenic emissions', *Geoscientific Model Development*, 5(6), pp. 1471–1492. doi: 10.5194/gmd-5-1471-2012.

Hallquist, M. *et al.* (2009) 'The formation, properties and impact of secondary organic aerosol: current and emerging issues', *Atmospheric Chemistry and Physics Discussions*, 9(1), pp. 3555–3762. doi: 10.5194/acpd-9-3555-2009.

Han, C. *et al.* (2018) 'Spatial and Temporal Trends of Number of Deaths Attributable to Ambient PM2.5 in the Korea', *Journal of Korean Medical Science*, 33.

Han, Z. *et al.* (2008) 'MICS-Asia II: Model intercomparison and evaluation of ozone and relevant species', *Atmospheric Environment*, 42(15), pp. 3491–3509. doi: https://doi.org/10.1016/j.atmosenv.2007.07.031.

Hayes, P. L. *et al.* (2015) 'Modeling the formation and aging of secondary organic aerosols in Los Angeles during CalNex 2010', *Atmospheric Chemistry and Physics*, 15(10), pp. 5773–5801. doi: 10.5194/acp-15-5773-2015.

Henze, D. K. *et al.* (2008) 'Global modeling of secondary organic aerosol formation from aromatic hydrocarbons: high- vs. low-yield pathways', *Atmos. Chem. Phys.*, 8(9), pp. 2405–2420. doi: 10.5194/acp-8-2405-2008.

Hodzic, A. *et al.* (2016) 'Rethinking the global secondary organic aerosol (SOA) budget: Stronger production, faster removal, shorter lifetime', *Atmospheric Chemistry and Physics*, 16(12), pp. 7917–7941. doi: 10.5194/acp-16-7917-2016.

Hodzic, A. and Jimenez, J. L. (2011) 'Modeling anthropogenically controlled secondary organic aerosols in a megacity: A simplified framework for global and climate models', *Geoscientific Model Development*, 4(4), pp. 901–917. doi: 10.5194/gmd-4-901-2011.

Hoek, G. *et al.* (2013) 'Long-term air pollution exposure and cardio-

respiratory mortality: A review', *Environmental Health: A Global Access Science Source*. doi: 10.1186/1476-069X-12-43.

Huang, X. *et al.* (2017) 'Chemical characterization and source identification of PM2.5 at multiple sites in the Beijing–Tianjin–Hebei region, China', *Atmos. Chem. Phys.*, 17(21), pp. 12941–12962. doi: 10.5194/acp-17-12941-2017.

Huangfu, P. and Atkinson, R. (2020) 'Long-term exposure to NO2 and O3 and all-cause and respiratory mortality: A systematic review and meta-analysis', *Environment International*. Elsevier Ltd. doi: 10.1016/j.envint.2020.105998.

Hwang, J. *et al.* (2020) 'Association between long-term exposure to air pollutants and cardiopulmonary mortality rates in South Korea', *BMC Public Health*, 20(1), p. 1402. doi: 10.1186/s12889-020-09521-8.

Jathar, S. H. *et al.* (2014) 'Unspeciated organic emissions from combustion sources and their influence on the secondary organic aerosol budget in the United States', *Proc Natl Acad Sci U S A*. 2014/07/09, 111(29), pp. 10473–10478. doi: 10.1073/pnas.1323740111.

Jeon, H. *et al.* (2015) 'The Characteristics of PM2.5 Concentration and Chemical Composition of Seoul Metropolitan and Inflow Background area in Korea Peninsula', *Journal of the Korean Society of Urban Environment*, 15(3), pp. 261–271. Available at: https://www.earticle.net/Article/A267061.

Jimenez, J. L. *et al.* (2009) 'Evolution of Organic Aerosols in the

Atmosphere', *Science*, 326(5959), pp. 1525–1529. doi: 10.1126/science.1180353.

Jo, D. S. *et al.* (2013) 'Effects of chemical aging on global secondary organic aerosol using the volatility basis set approach', *Atmospheric Environment*, 81, pp. 230–244. doi: https://doi.org/10.1016/j.atmosenv.2013.08.055.

Jo, D. S. *et al.* (2019) 'A simplified parameterization of isoprene-epoxydiol-derived secondary organic aerosol (IEPOX-SOA) for global chemistry and climate models: A case study with GEOS-Chem v11-02-rc', *Geoscientific Model Development*, 12(7), pp. 2983–3000. doi: 10.5194/gmd-12-2983-2019.

Jordan, C. *et al.* (2020) 'Investigation of factors controlling PM2.5 variability across the South Korean Peninsula during KORUS-AQ', *Elem Sci Anth*, 8, p. 28. doi: 10.1525/elementa.424.

Ju, M. J., Oh, J. and Choi, Y.-H. (2021) 'Changes in air pollution levels after COVID-19 outbreak in Korea', *Science of The Total Environment*, 750, p. 141521. doi: https://doi.org/10.1016/j.scitotenv.2020.141521.

Kang, H. G. *et al.* (2022) 'Volatility of Springtime ambient organic aerosol derived with thermodenuder aerosol mass spectrometry in Seoul, Korea', *Environmental Pollution*, 304(December 2021), p. 119203. doi: 10.1016/j.envpol.2022.119203.

KC, S. and Lutz, W. (2017) 'The human core of the shared

socioeconomic pathways: Population scenarios by age, sex and level of education for all countries to 2100', *Global Environmental Change*, 42, pp. 181–192. doi: https://doi.org/10.1016/j.gloenvcha.2014.06.004.

Kelly, F. J. and Fussell, J. C. (2012) 'Size, source and chemical composition as determinants of toxicity attributable to ambient particulate matter', *Atmospheric Environment*, 60, pp. 504–526. doi: https://doi.org/10.1016/j.atmosenv.2012.06.039.

Khan, A. *et al.* (2018) 'Airborne volatile aromatic hydrocarbons at an urban monitoring station in Korea from 2013 to 2015', *Journal of environmental management*, 209, pp. 525–538. doi: 10.1016/j.jenvman.2017.12.055.

Kim, H. *et al.* (2017) 'Sources and atmospheric processing of winter aerosols in Seoul, Korea: insights from real-time measurements using a high-resolution aerosol mass spectrometer', *Atmos. Chem. Phys.*, 17(3), pp. 2009–2033. doi: 10.5194/acp-17-2009-2017.

Kim, H. *et al.* (2021) 'Effects of long-term exposure to air pollution on all-cause mortality and cause-specific mortality in seven major cities of South Korea: Korean national health and nutritional examination surveys with mortality follow-up', *Environmental Research*, 192. doi: 10.1016/j.envres.2020.110290.

Kim, H., Zhang, Q. and Heo, J. (2018) 'Influence of intense secondary aerosol formation and long-range transport on aerosol chemistry and

properties in the Seoul Metropolitan Area during spring time: results from KORUS-AQ', *Atmospheric Chemistry and Physics*, 18(10), pp. 7149–7168. doi: 10.5194/acp-18-7149-2018.

Kim, H., Kim, Hyomi and Lee, J.-T. (2019) 'Spatial variation in lag structure in the short-term effects of air pollution on mortality in seven major South Korean cities, 2006–2013', *Environment International*, 125, pp. 595–605. doi: https://doi.org/10.1016/j.envint.2018.09.004.

Kim, J.-H. *et al.* (2018) 'Premature Deaths Attributable to Long-term Exposure to Ambient Fine Particulate Matter in the Republic of Korea', *J Korean Med Sci*, 33(37). Available at: https://doi.org/10.3346/jkms.2018.33.e251.

Kim, M. J. *et al.* (2015) 'Future ozone and oxidants change under the RCP scenarios', *Atmospheric Environment*, 101, pp. 103–115. doi: https://doi.org/10.1016/j.atmosenv.2014.11.016.

Kim, S. E. *et al.* (2020) 'Air quality co-benefits from climate mitigation for human health in South Korea', *Environment International*, 136. doi: 10.1016/j.envint.2020.105507.

Kim, S., Kim, H. and Lee, J.-T. (2019) 'Interactions between Ambient Air Particles and Greenness on Cause-specific Mortality in Seven Korean Metropolitan Cities, 2008–2016', *International Journal of Environmental Research and Public Health*, 16, p. 1866. doi: 10.3390/ijerph16101866.

Kim, Y. P. and Lee, G. (2018) 'Trend of Air Quality in Seoul: Policy and

Science', *Aerosol and Air Quality Research*, 18(9), pp. 2141–2156. doi: 10.4209/aaqr.2018.03.0081.

Kleinman, L. I. *et al.* (2008) 'The time evolution of aerosol composition over the Mexico City plateau', *Atmos. Chem. Phys.*, 8(6), pp. 1559–1575. doi: 10.5194/acp-8-1559-2008.

Lee, S. *et al.* (2022) 'A New Chemistry-Climate Model GRIMs-CCM: Model Evaluation of Interactive Chemistry-Meteorology Simulations', *Asia-Pacific Journal of Atmospheric Sciences*, 2(0123456789). doi: 10.1007/s13143-022-00281-6.

Lin, G., Penner, J. and Zhou, C. (2016) 'How will SOA change in the future?', *Geophysical Research Letters*, 43, p. n/a-n/a. doi: 10.1002/2015GL067137.

Lin, X., Trainer, M. and Liu, S. C. (1988) 'On the nonlinearity of the tropospheric ozone production', *Journal of Geophysical Research: Atmospheres*, 93(D12), pp. 15879–15888. doi: https://doi.org/10.1029/JD093iD12p15879.

Marais, E. A. *et al.* (2016) 'Aqueous-phase mechanism for secondary organic aerosol formation from isoprene: application to the southeast United States and co-benefit of SO2 emission controls', *Atmos. Chem. Phys.*, 16(3), pp. 1603–1618. doi: 10.5194/acp-16-1603-2016.

van Marle, M. J. E. *et al.* (2017) 'Historic global biomass burning emissions for CMIP6 (BB4CMIP) based on merging satellite observations

with proxies and fire models (1750–2015)', *Geosci. Model Dev.*, 10(9), pp. 3329–3357. doi: 10.5194/gmd-10-3329-2017.

McDuffie, E. *et al.* (2020) *A global anthropogenic emission inventory of atmospheric pollutants from sector-and fuel-specific sources (1970-2017): An application of the Community Emissions Data System (CEDS) Earth System Science Data Discussions*. doi: 10.5194/essd-2020-103.

Nault, B. A. *et al.* (2018) 'Secondary organic aerosol production from local emissions dominates the organic aerosol budget over Seoul, South Korea, during KORUS-AQ', *Atmos. Chem. Phys.*, 18(24), pp. 17769–17800. doi: 10.5194/acp-18-17769-2018.

Nault, B. A. *et al.* (2021) 'Secondary organic aerosols from anthropogenic volatile organic compounds contribute substantially to air pollution mortality', *Atmos. Chem. Phys.*, 21(14), pp. 11201–11224. doi: 10.5194/acp-21-11201-2021.

Ng, N. L. *et al.* (2007) 'Secondary organic aerosol formation from *m*-xylene, toluene, and benzene', *Atmos. Chem. Phys.*, 7(14), pp. 3909–3922. doi: 10.5194/acp-7-3909-2007.

NIER (2020) '2017 National Air Pollutants Emission', *Available at https://airemiss.nier.go.kr/ (accessed January 15, 2021).*

Oak, Y. J. *et al.* (2019) 'Evaluation of simulated O<inf>3</inf> production efficiency during the KORUS-AQ campaign: Implications for anthropogenic NO<inf>x</inf> emissions in Korea', *Elementa*, 7(1). doi:

10.1525/elementa.394.

Oak, Y. J. *et al.* (2022) 'Evaluation of Secondary Organic Aerosol (SOA) Simulations for Seoul, Korea', *Journal of Advances in Modeling Earth Systems*, 14(2). doi: 10.1029/2021MS002760.

Oak, Y. J. *et al.* (2023) 'Future air quality and premature mortality in Korea', *Science of The Total Environment*, 865, p. 161134. doi: https://doi.org/10.1016/j.scitotenv.2022.161134.

Oberdörster, G., Oberdörster, E. and Oberdörster, J. (2005) 'Nanotoxicology: an emerging discipline evolving from studies of ultrafine particles', *Environmental health perspectives*, 113(7), pp. 823–839. doi: 10.1289/ehp.7339.

Odum, J. R. *et al.* (1996) 'Gas/Particle Partitioning and Secondary Organic Aerosol Yields', *Environmental Science & Technology*, 30(8), pp. 2580–2585. doi: 10.1021/es950943+.

Pai, S. J. *et al.* (2020) 'An evaluation of global organic aerosol schemes using airborne observations', *Atmos. Chem. Phys.*, 20(5), pp. 2637–2665. doi: 10.5194/acp-20-2637-2020.

Park, J. *et al.* (2015) 'The Characteristics and Seasonal Variations of OC and EC for PM2.5 in Seoul Metropolitan Area in 2014', *Journal of Environmental Impact Assessment*, 24, pp. 578–592. doi: 10.14249/eia.2015.24.6.578.

Park, R. J. *et al.* (2003) 'Sources of carbonaceous aerosols over the

United States and implications for natural visibility', *Journal of Geophysical Research: Atmospheres*, 108(D12). doi: 10.1029/2002jd003190.

Park, R. J. *et al.* (2021) 'Multi-model intercomparisons of air quality simulations for the KORUS-AQ campaign', *Elementa: Science of the Anthropocene*, 9(1). doi: 10.1525/elementa.2021.00139.

Park, R. J. and Kim, S.-W. (2014) 'Air quality modeling in East Asia: present issues and future directions', *Asia-Pacific Journal of Atmospheric Sciences*, 50(1), pp. 105–120. doi: 10.1007/s13143-014-0030-9.

Park, S., Allen, R. and Lim, C.-H. (2020) 'A likely increase in fine particulate matter and premature mortality under future climate change', *Air Quality, Atmosphere & Health*, 13. doi: 10.1007/s11869-019-00785-7.

Peterson, D. *et al.* (2019) 'Meteorology influencing springtime air quality, pollution transport, and visibility in Korea', *Elem Sci Anth*, 7, p. 57. doi: 10.1525/elementa.395.

Philip, S. *et al.* (2014) 'Spatially and seasonally resolved estimate of the ratio of organic mass to organic carbon', *Atmospheric Environment*, 87, pp. 34–40. doi: 10.1016/j.atmosenv.2013.11.065.

Pio, C. *et al.* (2011) 'OC/EC Ratio Observations in Europe: Re-thinking the Approach for Apportionment between Primary and Secondary Organic Carbon', *Atmospheric Environment*, 45, pp. 6121–6132. doi: 10.1016/j.atmosenv.2011.08.045.

Porter, W. C., Safieddine, S. A. and Heald, C. L. (2017) 'Impact of

aromatics and monoterpenes on simulated tropospheric ozone and total OH reactivity', *Atmospheric Environment*, 169, pp. 250–257. doi: https://doi.org/10.1016/j.atmosenv.2017.08.048.

Pye, H. O. T. *et al.* (2010) 'Global modeling of organic aerosol: the importance of reactive nitrogen (NO_x and NO_3)', *Atmos. Chem. Phys.*, 10(22), pp. 11261–11276. doi: 10.5194/acp-10-11261-2010.

Pye, H. O. T. *et al.* (2021) 'Secondary organic aerosol association with cardiorespiratory disease mortality in the United States', *Nature Communications*, 12(1), p. 7215. doi: 10.1038/s41467-021-27484-1.

Reed, C. *et al.* (2016) 'Interferences in photolytic NO2 measurements: explanation for an apparent missing oxidant?', *Atmos. Chem. Phys.*, 16(7), pp. 4707–4724. doi: 10.5194/acp-16-4707-2016.

Ridley, D. A. *et al.* (2017) 'Causes and consequences of decreasing atmospheric organic aerosol in the United States', *Proceedings of the National Academy of Sciences of the United States of America*, 115(2), pp. 290–295. doi: 10.1073/pnas.1700387115.

Robinson, A. L. *et al.* (2007) 'Rethinking organic aerosols: semivolatile emissions and photochemical aging', *Science*. 2007/03/03, 315(5816), pp. 1259–1262. doi: 10.1126/science.1133061.

Saunois, M. *et al.* (2020) 'The Global Methane Budget 2000–2017', *Earth Syst. Sci. Data*, 12(3), pp. 1561–1623. doi: 10.5194/essd-12-1561-2020.

Schroeder, J. R. *et al.* (2020) 'Observation-based modeling of ozone

chemistry in the Seoul metropolitan area during the Korea-United States Air Quality Study (KORUS-AQ)', *Elementa: Science of the Anthropocene*. Edited by D. Helmig and J. Stutz, 8. doi: 10.1525/elementa.400.

Sellar, A. A. *et al.* (2019) 'UKESM1: Description and Evaluation of the U.K. Earth System Model', *Journal of Advances in Modeling Earth Systems*, 11(12), pp. 4513–4558. doi: https://doi.org/10.1029/2019MS001739.

Shaddick, G. *et al.* (2018) 'Data integration model for air quality: a hierarchical approach to the global estimation of exposures to ambient air pollution', *Journal of the Royal Statistical Society: Series C (Applied Statistics)*, 67(1), pp. 231–253. doi: https://doi.org/10.1111/rssc.12227.

Shilling, J. E. *et al.* (2009) 'Loading-dependent elemental composition of α-pinene SOA particles', *Atmos. Chem. Phys.*, 9(3), pp. 771–782. doi: 10.5194/acp-9-771-2009.

Shim, S. *et al.* (2020) 'Impact of Future Air Quality in East Asia under SSP Scenarios', *Atmosphere-Korea*, 30(4), pp. 439–454.

Silva, R. A. *et al.* (2016) 'The effect of future ambient air pollution on human premature mortality to 2100 using output from the ACCMIP model ensemble', *Atmospheric Chemistry and Physics*, 16(15), pp. 9847–9862. doi: 10.5194/acp-16-9847-2016.

Silva, R. A. *et al.* (2017) 'Future global mortality from changes in air pollution attributable to climate change', *Nature Climate Change*, 7(9), pp. 647–651. doi: 10.1038/nclimate3354.

Simpson, I. J. *et al.* (2020) 'Characterization, sources and reactivity of volatile organic compounds (VOCs) in Seoul and surrounding regions during KORUS-AQ', *Elementa: Science of the Anthropocene*. Edited by D. Helmig and J. Stutz, 8. doi: 10.1525/elementa.434.

Soares, A. R. and Silva, C. (2022) 'Review of Ground-Level Ozone Impact in Respiratory Health Deterioration for the Past Two Decades', *Atmosphere*. MDPI. doi: 10.3390/atmos13030434.

Stanier, C. O., Donahue, N. and Pandis, S. N. (2008) 'Parameterization of secondary organic aerosol mass fractions from smog chamber data', *Atmospheric Environment*, 42(10), pp. 2276–2299. doi: https://doi.org/10.1016/j.atmosenv.2007.12.042.

Thornhill, G. *et al.* (2021) 'Climate-driven chemistry and aerosol feedbacks in CMIP6 Earth system models', *Atmospheric Chemistry and Physics*, 21(2), pp. 1105–1126. doi: 10.5194/acp-21-1105-2021.

Travis, K. R. *et al.* (2022) 'Limitations in representation of physical processes prevent successful simulation of PM2.5 during KORUS-AQ', *Atmos. Chem. Phys.*, 22(12), pp. 7933–7958. doi: 10.5194/acp-22-7933-2022.

Turnock, S. T. *et al.* (2020) 'Historical and future changes in air pollutants from CMIP6 models', *Atmos. Chem. Phys.*, 20(23), pp. 14547–14579. doi: 10.5194/acp-20-14547-2020.

Turpin, B. J. and Huntzicker, J. J. (1995) 'Identification of secondary organic aerosol episodes and quantitation of primary and secondary organic

aerosol concentrations during SCAQS', *Atmospheric Environment*, 29(23), pp. 3527–3544. doi: https://doi.org/10.1016/1352-2310(94)00276-Q.

Ulbrich, I. M. *et al.* (2009) 'Interpretation of organic components from Positive Matrix Factorization of aerosol mass spectrometric data', *Atmos. Chem. Phys.*, 9(9), pp. 2891–2918. doi: 10.5194/acp-9-2891-2009.

Wang, J. *et al.* (2016) 'Historical Trends in PM2.5-Related Premature Mortality during 1990-2010 across the Northern Hemisphere', *Environmental Health Perspectives*, 125. doi: 10.1289/EHP298.

Wang, L. *et al.* (2021) 'Characteristics of wintertime VOCs in urban Beijing: Composition and source apportionment', *Atmospheric Environment: X*, 9, p. 100100. doi: https://doi.org/10.1016/j.aeaoa.2020.100100.

van der Werf, G. R. *et al.* (2010) 'Global fire emissions and the contribution of deforestation, savanna, forest, agricultural, and peat fires (1997–2009)', *Atmos. Chem. Phys.*, 10(23), pp. 11707–11735. doi: 10.5194/acp-10-11707-2010.

Woo, J.-H. *et al.* (2012) 'Development of an anthropogenic emissions processing system for Asia using SMOKE', *Atmospheric Environment*, 58, pp. 5–13. doi: https://doi.org/10.1016/j.atmosenv.2011.10.042.

Woo, J.-H. *et al.* (2020) 'Development of the CREATE Inventory in Support of Integrated Climate and Air Quality Modeling for Asia', *Sustainability*, 12, p. 7930. doi: 10.3390/su12197930.

World Health Organization (2003) 'Health Aspects of Air Pollution with

Particulate Matter , Ozone and Nitrogen Dioxide', *Report on a WHO Working Group Bonn, Germany 13–15 January 2003*. Copenhagen : WHO Regional Office for Europe, p. 98. Available at: http://www.euro.who.int/__data/assets/pdf_file/0005/112199/E79097.pdf.

Wu, C. and Yu, J. Z. (2018) 'Evaluation of linear regression techniques for atmospheric applications: the importance of appropriate weighting', *Atmos. Meas. Tech.*, 11(2), pp. 1233–1250. doi: 10.5194/amt-11-1233-2018.

Xing, L. *et al.* (2013) 'Seasonal and spatial variability of the OM/OC mass ratios and high regional correlation between oxalic acid and zinc in Chinese urban organic aerosols', *Atmos. Chem. Phys.*, 13(8), pp. 4307–4318. doi: 10.5194/acp-13-4307-2013.

Xu, J. *et al.* (2021) 'Estimation of ambient PM2.5-related mortality burden in China by 2030 under climate and population change scenarios: A modeling study', *Environment International*, 156. doi: 10.1016/j.envint.2021.106733.

Yorifuji, T. *et al.* (2015) 'Health Impact Assessment of PM10 and PM2.5 in 27 Southeast and East Asian Cities', *Journal of occupational and environmental medicine / American College of Occupational and Environmental Medicine*, 57, pp. 751–756. doi: 10.1097/JOM.0000000000000485.

Zhai, S. *et al.* (2023) 'Coarse particulate matter air quality in East Asia: implications for fine particulate nitrate', *EGUsphere*, 2023, pp. 1–18. doi:

10.5194/egusphere-2022-1485.

Zhang, J. *et al.* (2006) 'Secondary Organic Aerosol Formation from Limonene Ozonolysis: Homogeneous and Heterogeneous Influences as a Function of NOx', *The Journal of Physical Chemistry A*, 110(38), pp. 11053–11063. doi: 10.1021/jp062836f.

Zhang, Q. *et al.* (2007) 'Ubiquity and dominance of oxygenated species in organic aerosols in anthropogenically-influenced Northern Hemisphere midlatitudes', *Geophysical Research Letters*, 34(13). doi: 10.1029/2007gl029979.

Zhang, X. *et al.* (2014) 'Influence of vapor wall loss in laboratory chambers on yields of secondary organic aerosol', *Proceedings of the National Academy of Sciences*, 111(16), pp. 5802 LP – 5807. doi: 10.1073/pnas.1404727111.

Zheng, B. *et al.* (2018) 'Trends in China's anthropogenic emissions since 2010 as the consequence of clean air actions', *Atmospheric Chemistry and Physics Discussions*. doi: 10.5194/acp-2018-374.

Zhou, W. *et al.* (2020) 'A review of aerosol chemistry in Asia: insights from aerosol mass spectrometer measurements', *Environ Sci Process Impacts*. 2020/07/17, 22(8), pp. 1616–1653. doi: 10.1039/d0em00212g.

국문 초록

대류권 오존(O_3)과 초미세먼지($PM_{2.5}$)와 같은 대기오염물질에 장기간 노출될 경우 심혈관계 및 호흡계 질환이 유발되는 것으로 알려져 있으며, 1990년대 후반부터 국내 대기질을 개선하기 위한 정부의 노력으로 O_3과 $PM_{2.5}$의 전구체 배출량이 꾸준히 감소해 왔다. 하지만 2차 생성되는 O_3과 $PM_{2.5}$의 농도 변화는 전구체의 농도와 다른 양상을 보이고 있다 (Kim and Lee, 2018). 따라서 본 연구는 국내 대기오염물질의 2차 생성 과정에 대한 이해를 높이기 위해 주요 전구 물질인 휘발성유기화합물(VOCs)의 기체상 화학 과정과 입자상 유기에어로졸(OA) 생성 및 소멸 과정에 대한 분석을 수행하였다. 우리나라를 포함한 동아시아에서는 다양한 VOCs 중에서도 반응성이 높은 방향족 화합물의 농도가 높게 관측됨에 따라, 먼저 방향족 VOCs의 기체상 화학 반응이 국내 O_3 생성에 미치는 영향을 조사하였다. 3차원 화학수송모델(CTM)인 GEOS-Chem에 고도화된 방향족 화학 메커니즘을 적용한 결과, 국내 O_3 농도가 13% 증가하는 것을 확인하였다. 또한, 업데이트된 메커니즘으로 모의한 O_3 생성 효율(OPE)을 관측 기반의 박스모델과 비교 검증한 결과, 질소산화물(NO_x)이 기존 배출량 인벤토리에서 과소평가되었음을 확인하였다. 추가적인 민감도 테스트를 통해 국내 NO_x 배출량을 30% 감축했을 때 도심 지역에서는 지표면 O_3 농도가 증가하지만, NO_x와 VOCs 배출 감축을 동시에 성공적으로 수행할 경우, 지표 O_3이 전국적으로

감소하는 것을 알 수 있었다. VOCs의 산화 산물은 추가적인 화학 과정을 거쳐 O_3뿐만 아니라 $PM_{2.5}$를 이루는 주요 구성 성분인 2차 유기 에어로졸(SOA)을 생성하게 된다. 본 연구에서는 GEOS-Chem을 사용하여 다양한 SOA 모의 방법을 활용하여 비교 검증을 수행하여 국내에서 관측된 SOA의 계절별 생성 및 소멸 특성을 조사하였다. 그 결과, 국내 도심 지역에서 나타나는 SOA의 광화학적 특성을 가장 적절하게 모의하기 위해 모델 내 준휘발성유기화합물(S/IVOCs) 전구체에 대한 고려가 필요하며, SOA의 화학적 노화 과정(functionalization; 작용기화에 의한 휘발성 감소 및 질량 증가)이 중요한 요소임을 확인하였다. 마지막으로 본 연구에서는 기체상/입자상 유기화학 과정에 대한 모델 검증을 바탕으로 SSP(Shared Socioeconomic Pathways) 미래 시나리오 하에서 국내 대기질 변화를 모의하고, 이에 따른 심혈관계 조기사망에 대한 건강 영향 평가를 수행하였다. 업데이트된 방향족 화학과정과 최적화된 SOA 모의 방법을 적용하여 현재(2019), 가까운 미래(2045), 먼 미래(2095)의 오염물질 농도와, 국내 코호트 및 역학 연구 기반의 농도 반응 함수(CRF)를 활용하여 대기오염으로 인한 조기사망자수를 추정하였다. SSP1 시나리오 하에서 미래 인위배출량이 크게 감소하면서 국내 대기질이 상당히 개선될 것이며, 이로 인한 심혈관계 조기사망자수는 2095년에 95% 감소하는 것으로 나타났다. 하지만 미래 $PM_{2.5}$ 구성 성분들의 상대적인 기여도가 변하면서, 식생 기원 SOA(BSOA)의 농도가

높은 지역은 대기오염에 더욱 취약해질 것으로 예상된다. SSP3 시나리오에서는 대기질이 현재와 비슷할 것으로 예상되며, 대기오염으로 인한 조기사망은 인구 변화의 추세를 따라 2045년에는 80% 증가하지만 2095년에는 현재에 비해 22% 감소할 것으로 보인다. 하지만 BSOA 농도의 증가로 SOA에 의한 조기사망자수는 ~20% 증가하는 것으로 나타났다.

주요어: 화학수송모델, 휘발성유기화합물, 오존, 유기에어로졸, 초미세먼지, 대기질, 조기사망률
학 번: 2016-23700